NAVAL POSTGRADUATE SCHOOL
Monterey, California

THESIS

AN EXPERIMENTAL INVESTIGATION OF FLAPPING WING AERODYNAMICS IN MICRO AIR VEHICLES

by

Christopher John Bradshaw

June 2003

Thesis Advisor: Kevin D Jones
Second Reader: Max F Platzer

Approved for public release; distribution is unlimited.

THIS PAGE INTENTIONALLY LEFT BLANK

REPORT DOCUMENTATION PAGE	Form Approved OMB No. 0704-0188

1. AGENCY USE ONLY *(Leave blank)*	2. REPORT DATE	3. REPORT TYPE AND DATES COVERED
	June 2003	Master's Thesis

4. TITLE AND SUBTITLE: An Experimental Investigation of Flapping Wing Aerodynamics in Micro Air Vehicles	5. FUNDING NUMBERS
6. AUTHOR(S) Christopher John Bradshaw	
7. PERFORMING ORGANIZATION NAME(S) AND ADDRESS(ES) Naval Postgraduate School Monterey, CA 93943-5000	8. PERFORMING ORGANIZATION REPORT NUMBER
9. SPONSORING / MONITORING AGENCY NAME(S) AND ADDRESS(ES) N/A	10. SPONSORING / MONITORING AGENCY REPORT NUMBER

11. SUPPLEMENTARY NOTES The views expressed in this thesis are those of the author and do not reflect the official policy or position of the Department of Defense or the U.S. Government.

12a. DISTRIBUTION / AVAILABILITY STATEMENT Approved for public release; distribution is unlimited	12b. DISTRIBUTION CODE

13. ABSTRACT *(maximum 200 words)*

Flapping-wing propulsion was studied experimentally through Laser Doppler Velocimetry. Measurements were both time-averaged and unsteady, and were conducted on a Micro-Air Vehicle (MAV) model developed at NPS by Professors Max Platzer and Kevin Jones. The objective of this work was to further understanding of the aerodynamics of flapping-wing propulsion. In specific, this study examined separation control on the leading fixed wing due to entrainment by the trailing flapping wings. Further, a study of wake topology examined differences between the optimal and off-optimal cases. Experimental studies took place in the NPS 5' x 5' low speed wind tunnel. The model was supported on a test stand and LDV measurements of the flow field were taken. Studies were made at varying freestream velocities, angles of attack, and flapping frequencies. The test stand was instrumented with force balances to show forces in both the streamwise and vertical directions.

14. SUBJECT TERMS Flapping-wing, Micro-Air Vehicle, Low Reynolds Number, Laser Doppler Velocimetry	15. NUMBER OF PAGES 111
	16. PRICE CODE

17. SECURITY CLASSIFICATION OF REPORT	18. SECURITY CLASSIFICATION OF THIS PAGE	19. SECURITY CLASSIFICATION OF ABSTRACT	20. LIMITATION OF ABSTRACT
Unclassified	Unclassified	Unclassified	UL

NSN 7540-01-280-5500 Standard Form 298 (Rev. 2-89) Prescribed by ANSI Std. 239-18

THIS PAGE INTENTIONALLY LEFT BLANK

Approved for public release; distribution is unlimited.

AN EXPERIMENTAL INVESTIGATION OF FLAPPING WING AERODYNAMICS IN MICRO AIR VEHICLES

Christopher John Bradshaw
Ensign, United States Naval Reserve
B.S., Georgia Institute of Technology, 2002

Submitted in partial fulfillment of the
requirements for the degree of

MASTER OF SCIENCE IN AERONAUTICAL ENGINEERING

from the

NAVAL POSTGRADUATE SCHOOL
June 2003

Author: Christopher John Bradshaw

Approved by: Dr. Kevin D Jones
Thesis Advisor

Dr.Max F. Platzer
Second Reader

Dr. Max F. Platzer
Chairman, Department of Aeronautics and Astronautics

THIS PAGE INTENTIONALLY LEFT BLANK

ABSTRACT

Flapping-wing propulsion was studied experimentally through Laser Doppler Velocimetry. Measurements were both time-averaged and unsteady, and were conducted on a Micro-Air Vehicle (MAV) model developed at NPS by Professors Max Platzer and Kevin Jones. The objective of this work was to further understanding of the aerodynamics of flapping-wing propulsion. In specific, this study examined separation control on the leading fixed wing due to entrainment by the trailing flapping wings. Further, a study of wake topology examined differences between the optimal and off-optimal cases. Experimental studies took place in the NPS 5′ x 5′ low speed wind tunnel. The model was supported on a test stand and LDV measurements of the flow field were taken. Studies were made at varying freestream velocities, angles of attack, and flapping frequencies. The test stand was instrumented with force balances to show forces in both the streamwise and vertical directions.

THIS PAGE INTENTIONALLY LEFT BLANK

TABLE OF CONTENTS

THIS PAGE INTENTIONALLY LEFT BLANK

LIST OF SYMBOLS

c mean geometric chord of the flapping wing

U streamwise velocity component, normalized by V_∞, 9.2 fps

V vertical velocity component, normalized by V_∞, 9.2 fps

X streamwise location, positive downstream, X=0 is at the flapping wings' trailing edge.

Y spanwise location, positive to port, origin on the MAV's centerline

Z vertical direction, positive up, origin at the fixed wing's trailing edge

THIS PAGE INTENTIONALLY LEFT BLANK

LIST OF FIGURES

THIS PAGE INTENTIONALLY LEFT BLANK

LIST OF TABLES

THIS PAGE INTENTIONALLY LEFT BLANK

ACKNOWLEDGEMENTS

The author would like to extend his sincere appreciation to Professor Kevin Jones for his enthusiastic instruction and technical advice, and to Professor Garth Hobson for his shared expertise in the mysterious world of TSI hardware and software.

THIS PAGE INTENTIONALLY LEFT BLANK

I. INTRODUCTION

A. OVERVIEW

The purpose of this paper is to examine the unsteady flow around a pair of counter-phase pitching and plunging airfoils used to power a Micro-Air Vehicle. At low Reynolds numbers, flapping wings have the potential to be a more efficient means of propulsion for small, lightweight aircraft than either conventional propellers or rotary-wings. The hope is that a better understanding of the flow field about the flapping wings will allow for more efficient design and application of this ripening technology.

Experimental observations were made in the NPS low-speed in-draft wind tunnel with a 5′ x 5′ test section, and a TSI two-channel Laser Doppler Anemometer.

B. BACKGROUND

The obviousness of effective propulsion via flapping wings was regarded as early as Icarus and Daedalus, and perhaps earlier, though with sometime disastrous if fictional results. With regard to a more factual approach, any child can recognize that a variety of birds and insects propel themselves through the air via flapping wings. Indeed, in the early days of human flight, a number of attempts were made to emulate the flapping of the birds as a means of flight; most meeting with singularly Icaran results.

Current wisdom would suggest that these early attempts failed for any number of reasons but especially the structural weight of large man-carrying machines that must also flap their primary lifting surfaces. The flapping wing MAV designed by Professors Platzer and Jones and examined herein addresses this problem in a unique fashion. First, being a micro-air vehicle, the machine is penalized neither by the weight of a pilot nor by a very large structural weight. Even so, it is not the primary lifting surface that is pitched and plunged to achieve the flapping motion, but rather two smaller trailing edge counter-phase flappers. The purpose of this experiment was to examine experimentally the flow field about those two flapping wings and the effect of their flapping on the flow over the main wing.

C. OBJECTIVES

The ostensible goal of this work was to contribute to the body of knowledge being developed at NPS and elsewhere with regard to flapping-wing propulsion. In specific, the primary goal was to develop a time-unsteady model of the flow field about the trailing edge pitching and plunging device as developed by Professors Platzer and Jones. Special attention was paid to flow entrainment about the leading fixed wing with respect to stall delay. Also of interest were the variations in wake patterns among off- and on-optimal cases. To this end, a procedure was developed using frequency-resolved LDV data to examine the flow around the full-scale device in a wind tunnel environment.

III. EXPERIMENTAL APPROACH

A. MODELS

All models studied in this report are the product of years of analysis and experimentation by Professor Kevin Jones, who is responsible for their construction as well as that of the hardware used to mount and instrument the models.

1. Main Wing Section

Though absent for much of the experimental work, the main wing is crucial in generating the lift required to hold the operational MAV aloft. Consequently, the fixed wing is added to the wind-tunnel model in order to examine interaction between itself and the trailing edge flapping wings.

The main wing's frame is composed entirely of hand-carved balsa and carbon fiber assembled with glue. The skin is of Japanese tissue paper. The fuselage houses the motor, transmission, battery and radio gear in the operational model, but only the motor and transmission in the wind tunnel model.

The span of the main wing is slightly wider than that of the flapping wings at 10.5" with a mean geometric chord of 5.5" and absent both taper ratio and sweep. The main wing also has 8.5° of dihedral.

The main wing's airfoil section might ideally be infinitely thin; however, structural considerations deny this option [cf. Ref 2].

2. Flapping Wings

The flapping wings are powered by a small electric motor run on an external power supply for the purpose of this experiment. The plunging motion of the flapping wings is enforced by the motor's rotation, but the pitching motion is aeroelastic in nature and is limited by the stiffness in the flexible wing mounts. The wings move in counterphase to cancel out the inertial and aerodynamic effects of a single wing moving up and down.

The flapping wings are identical in construction, each having a chord of 1.5" and a span of 9.75". The leading edge is a balsa dowel. The wing's surface is of microfilm interspersed at intervals with chordwise battens. The plunging amplitude, from the centerline to top-dead-center, is 0.6" or 0.4 chordlengths, with a mean separation of 3.2".

Figure 1. Side View of Flapping Wing Model

3. Test Mount

The stand upon which the model is placed is isolated from wind tunnel vibration by being attached not to the floor of the tunnel, but through a covered hole in the floor to the more stationary structure beneath. This test stand is faired into the wind by being shaped like a symmetric airfoil, and is outfitted with sensors to resolve lift and drag in the stability axes, i.e., in the streamwise and vertical directions. The mount also allows the model to be rotated about the spanwise or "pitch" axis, enabling the model to be studied at varying angles of attack.

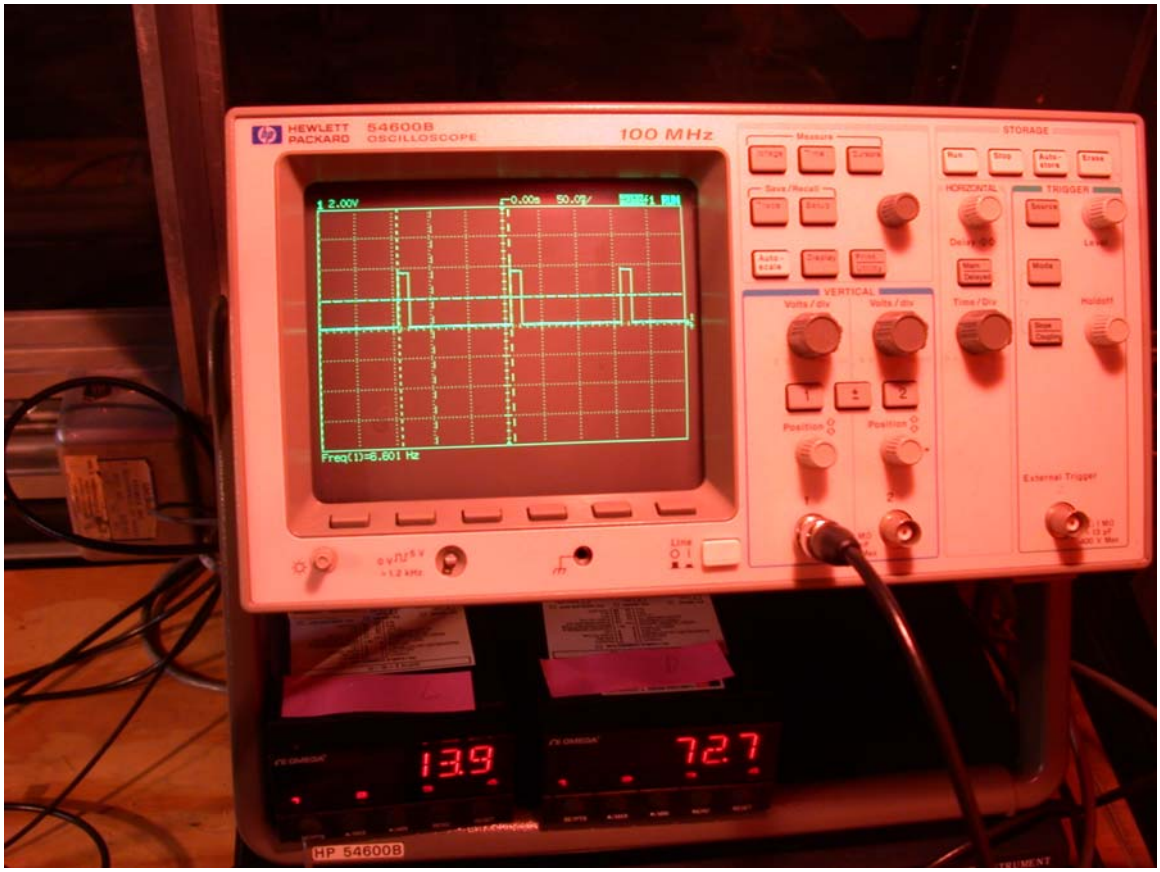

Figure 2. Oscilloscope Demonstrating Square-Wave Signal with Lift and Drag Gauges Beneath

B. TEST EQUIPMENT

1. Wind Tunnel

The experiments referred to herein were each conducted in the NPS low speed in-draft wind tunnel. This tunnel ingests air from within the building through a 15′ square intake. Following a 9:1 contraction, the flow enters a 5′ square test section. Flow speed is modulated by a constant-speed, variable-pitch electric fan. The fan is suspended on rubberized mounts to minimize vibration in the test section. Further, to reduce swirl and turbulence in the tunnel, honeycomb screens have been placed both before and after the test section, though the downstream screens do more to protect the fans from runaway models than to straighten the flow.

2. Laser Doppler Velocimeter

The primary technique used to observe the velocities in the flow field about the MAV was laser Doppler velocimetry. Specifically, a TSI two-channel LDV system with a single probe was used. The streamwise component of the flow was observed via the blue channel at 1.92×10^{-5} in (488 nm) wavelength, and the vertical component via the green channel at a wavelength of 2.03×10^{-5} in (514.5 nm). Both colored beams were phase shifted by the Bragg cell at a frequency of 1 MHz. For more detail on the mechanics of how an LDV systems measures flow velocity, please see Lund, Appendix C.

Figure 3. TSI Laser

The probe was fixed to a VP-9000 three-dimensional traverse, which was controlled remotely via a Windows PC running TSI's Flow Information Display (FIND) or PACE software.

The FIND software, as its name implies, also interpreted and displayed velocity data from the LDV system. As well, FIND allowed the user to tweak various settings of his equipment in real time. Parameters under the PC's control included the frequency of the phase shift, and the frequency band of interest. PACE is a very similar program, except that it incorporates the use of the Rotating Machinery Resolver, explicated below.

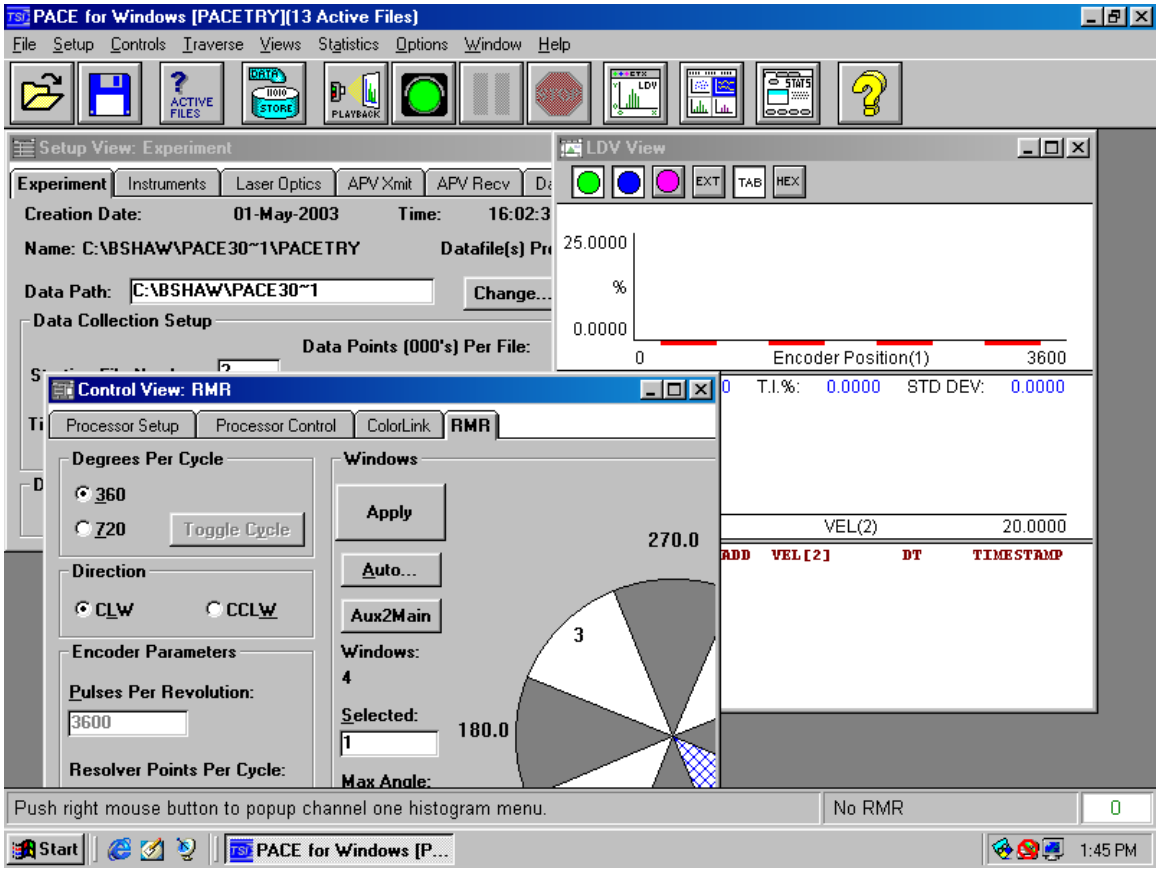

Figure 4. TSI's PACE for Windows GUI

Seeding was generated via a theatrical fog machine using Rosco non-toxic smoke fluid. This method generated particles of between 1×10^{-5}" and 2.5×10^{-3}" diameter [cf. Ref 8].

One of the black boxes of the LDV system was a Rotating Machinery Resolver (RMR). This machine acquired a lock on the period of revolution of the MAV's flapping via a square wave. A shaft encoder was built to generate the wave each time the wings returned to their centerline position. Due to this rotary technology, velocities measured at different sectors in the flapping cycle could be measured and stored independently of each other. In this method, the flow field about the flapping wings need not be measured on a time-averaged basis. Each portion of the cycle can be studied separately and with relation to the others.

C. SETUP

When fully assembled, the test apparatus functionality may be represented by the flow chart in the figure below.

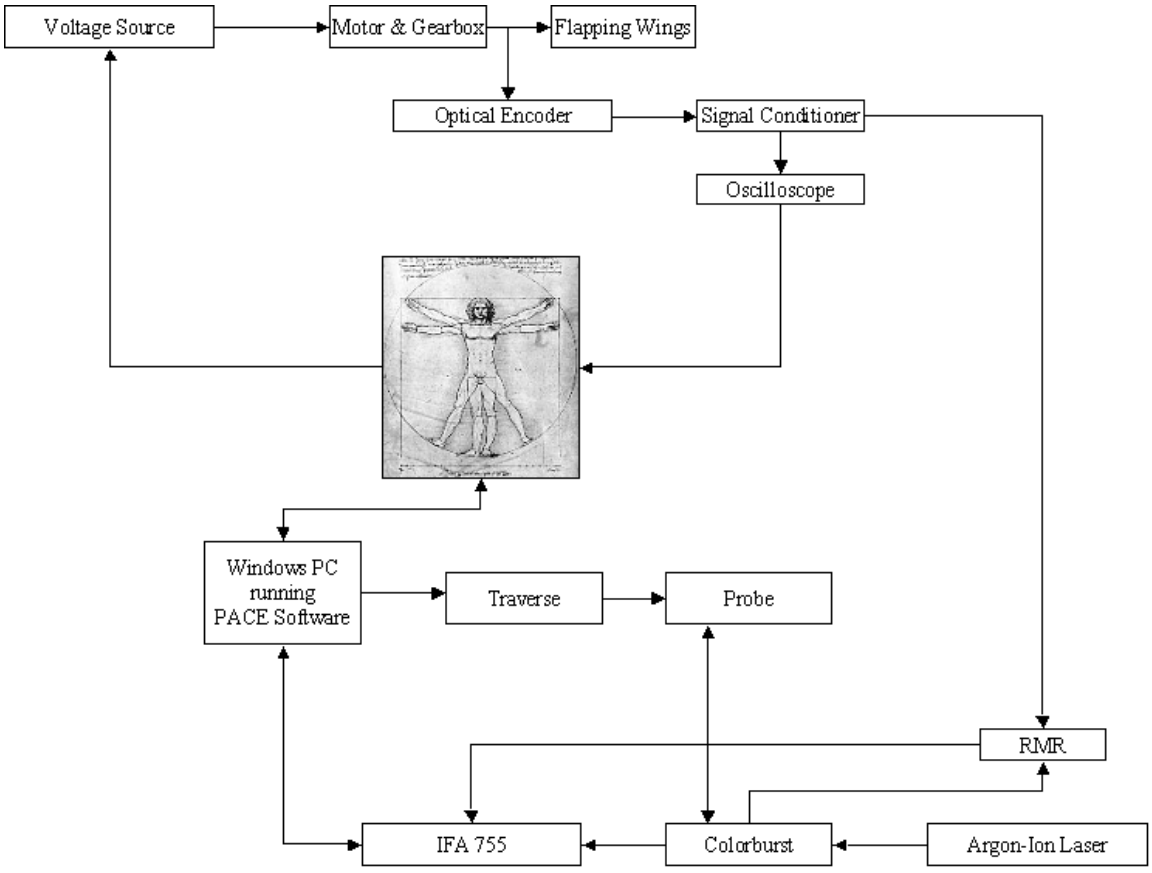

Figure 5. Flow Chart of Experimental Instrumentation

An explanation of the flow chart is in order. Beginning in the upper left, the Voltage source, controlled by the operator, output a DC current used to power the MAV. For the three frequencies used in the experiment, i.e., 25.6, 32, and 38.4Hz, the Voltages needed by the motor were

7.9, 9.8, and 11.8 Volts respectively. The motor referred to here is the second, more powerful 12V motor used for the bulk of the experiment.

The rotation of the electric motor turned the crankshaft connected to the flapping wings. As well, the same shaft turned the optical encoder, a device built by Prof. Jones in which a disk with a single slot rotates between an LED and a photocell. Each rotation of the disk allowed a pulse of light to pass through the slot and to be intercepted by the photocell. This cell then emitted a weak electrical current that was transmitted to the signal conditioner.

The signal conditioner, upon receiving the weak electric pulse of the photocell, emitted the leading edge of a short, 5V square wave. This step was necessary because the RMR, described above, had very stringent requirements about the signal it could use to acquire a phase lock. It needed a 50Ω TTL signal.

The square wave was also sent to an oscilloscope, from which the operator read the frequency of oscillation of the flapping wings and adjusted the voltage input accordingly. Given a constant voltage, the MAV model was quite good at holding a frequency, to within 0.25Hz or about 0.8%.

The newly conditioned signal was then sent to the RMR. The RMR used the square wave to acquire a phase locked loop. By this method, the RMR can know what part of the cycle it is in, even though it only receives one rising-edge input per cycle. That is to say that the machine determined the time that the MAV exhausted in one cycle and divided it into 360 parts--each representing one degree of

rotation. When it received the signal from the Colorburst that a particle's velocity had been measured by the LDV, the RMR made a note of the position where the MAV was in its cycle when the velocity was measured. The RMR then sent a signal to the IFA to flag that velocity with a number indicating the number of degrees elapsed between the rising edge and the particle's passing through the control volume.

The Intelligent Flow Analyzer, model 755, turned the signal from the Colorburst into a form usable by the PC and transmitted the same to the PC where it was recorded by the PACE software.

The Colorburst was yet another black box in the LDV system. Colorburst incorporated the phase shifter that increased the velocity of particles in the flow relative to the lines of interference in the probe volume, allowing measurement of negative velocities. Its primary function, however, was to receive and digitize data received from the probe in the form of fiber-optically transmitted pulses of reflected light.

The Argon-Ion Laser, of course, generated the laser beams used to create the probe volume in the flow. Although it is capable of using much more power, it was found that the best data rate was achieved by using 3.4 BTU/hr (.99 Watt).

The PC was very busy. Via the Windows-based PACE software, it was able to control every aspect of the LDV system. Using inputs from the operator, the PC controlled the settings of the Colorburst and received velocity and frequency data from the IFA. Following a matrix created by the operator, the PC was able to determine when enough data

had been collected at a given point in the flow and to move the traverse to the next indicated point. The power held by the computer over the LDV system enabled the experiment to be almost completely automated after some initial setup. However, it was found to behoove the operator to stay nearby and monitor the experiment's progress, if for nothing more than to be certain that the flow seeding was properly adjusted.

D. PROCEDURE

In the course of designing the experiment, certain decisions appeared, and forced themselves to be dealt with. In the interest of scientific purity, the following paragraphs will detail the reasons for most of the more important decisions.

Though it is not known how three dimensional the wake is about the flapping wings, that three-dimensionality is well beyond the scope of this thesis, not only because the LDV in the low-speed wind tunnel has only two components, but also, as cursory inspection of the appendices will indicate, even the narrow scope that was applied to this study has generated massive amounts of data with which to be reckoned and written intelligently about. Ergo, the spanwise location at which to study the flow field became a concern. At first, the centerline might seem a logical place to examine a wake, but the location of the test stand belied this theory. A simple spanwise survey of the flow behind the model generated the following results.

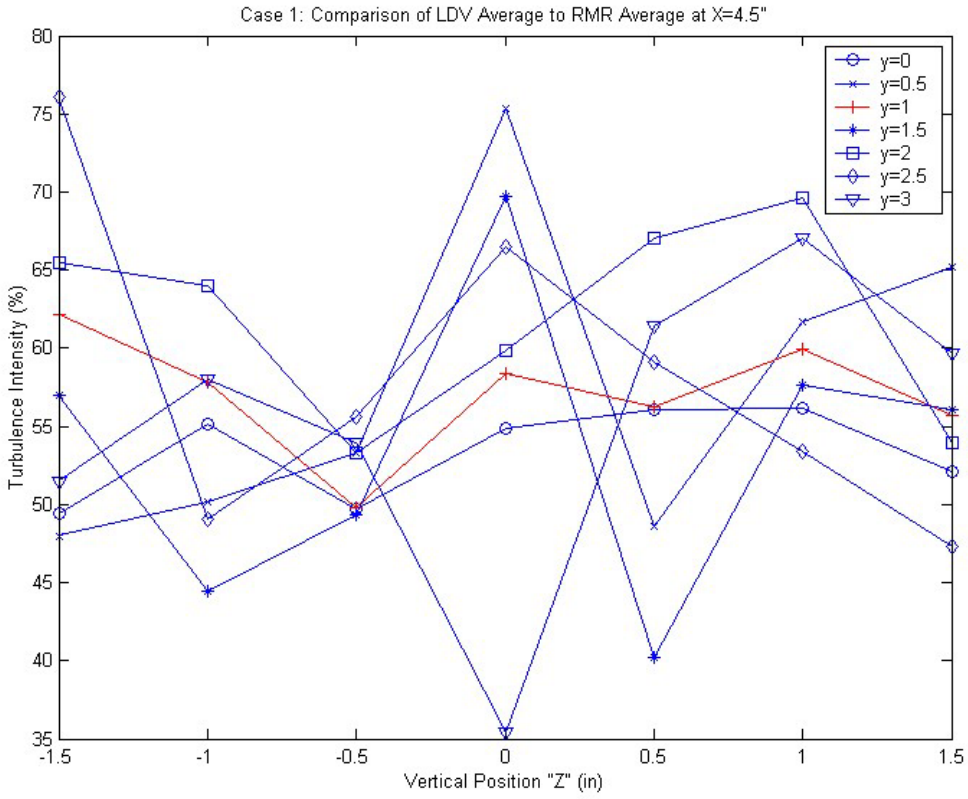

Figure 6. Spanwise Survey of Turbulence Intensity

A number of parameters were examined and proved inconclusive, including mean velocity, standard deviation, and seeding effectiveness. These results tended to indicate that the wake was indeed quite uniform, however, the decision had to be made and it was finally based upon the regularity of the turbulence intensity at 1" to port of the centerline.

That done, a grid in the remaining two dimensions was to be designed. It was decided that the portions closer to the MAV should be spaced at ¼ inch and that the outer nodes should be spaced at ½ inch. Five columns were chosen: the

first one chord-length before the flapping wing's leading edge, the second immediately before the leading edge, the third immediately aft of the flapping wing's trailing edge, the fourth one chord-length downstream of that, and yet a fifth two more chord-lengths downstream. The grid is illustrated in figure 7.

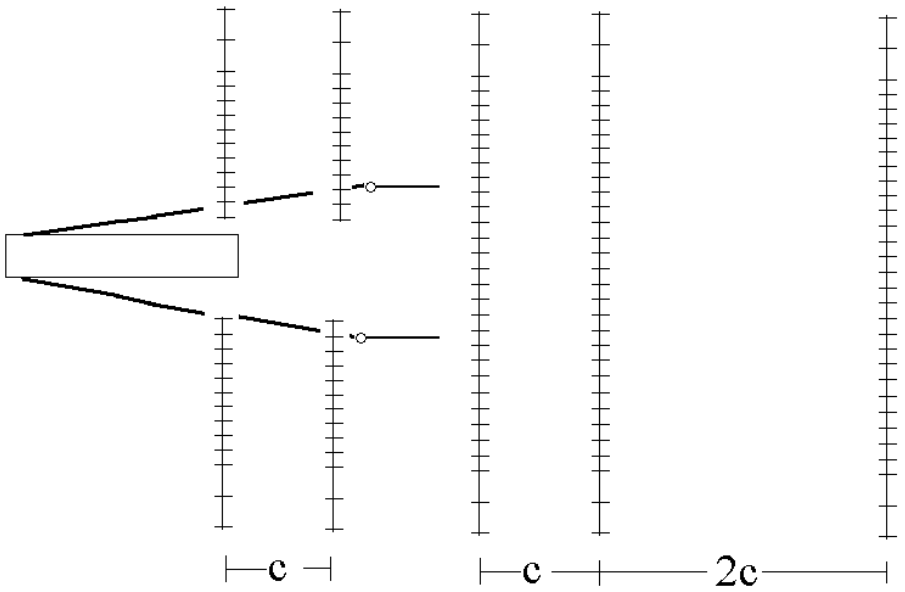

Figure 7. Experimental Grid

See the appendices for vector plots of the velocity at each node and that velocity's variation throughout the cycle, normalized by the freestream velocity.

The next call to be made involved which cases to examine. Consultation with my advisor yielded the cases described in Table 1.

Table 1. Cases under Examination

Test Case	AOA (deg)	Vinf (fps)	Frequency(Hz)	Configuration
1	15	9.2	32	Wing attached
2	15	9.2	0	Wing attached
3	15	9.2	32	No fixed wing
4	0	9.2	32	No fixed wing
5	0	9.2	38.4	No fixed wing
6	0	9.2	25.6	No fixed wing

One final, major question remained, and this was to determine how much time was spent and/or wasted gathering necessary or extraneous data points. That is to say, exactly how many velocities need to be measured by the LDV before one can say one has indeed measured the velocity. In the static case, this was quite simple since 1000 points can be gathered quite quickly, but for the RMR, each case is divided into 72 sections, and to wait for 72,000 points at each of 78 nodes in 5 cases could take an eternity. Consequently, following consultation with Professors Chandrasekhar and Hobson, a study was devised whereby the relative merits of differing numbers of data points could be compared. The table you see below was the result, and I am thrilled to report that the result was that only 3600 points (or 50 points per 5° of arc) were found to be necessary.

Table 2. Necessary Number of Data Points

Avg pts/5deg	Min Points/5deg	TI (%)	StDev
50	25	3.12	0.19
100	50	2.93	0.37
200	100	3.16	0.28
400	200	3.17	0.31

IV. RESULTS

A. FLOW FORWARD OF THE FLAPPING WINGS

As you will no doubt notice upon inspection of the plots, examination of the flow ahead of the flapping wings produced some rather fascinating results. Witness Figure 8. Here, the ‘x’s represent the air’s horizontal velocity component immediately upstream of the flapping wing’s leading edge, while the ‘o’s are one chord length upstream of that. In less than an inch and a half, the flow has accelerated from slightly above freestream speed to almost half again the same speed. The lack of definition in the flow over the upper surface is due, as has no doubt been noticed, to the absence of points within nearly two inches of the model’s centerline. The dihedral of the fixed wing prevented the LDV’s probe volume from descending closer to the wing’s surface. This was a problem for both Cases 1 and 2, though for the final four cases, the wing was removed and the probe allowed to descend significantly farther.

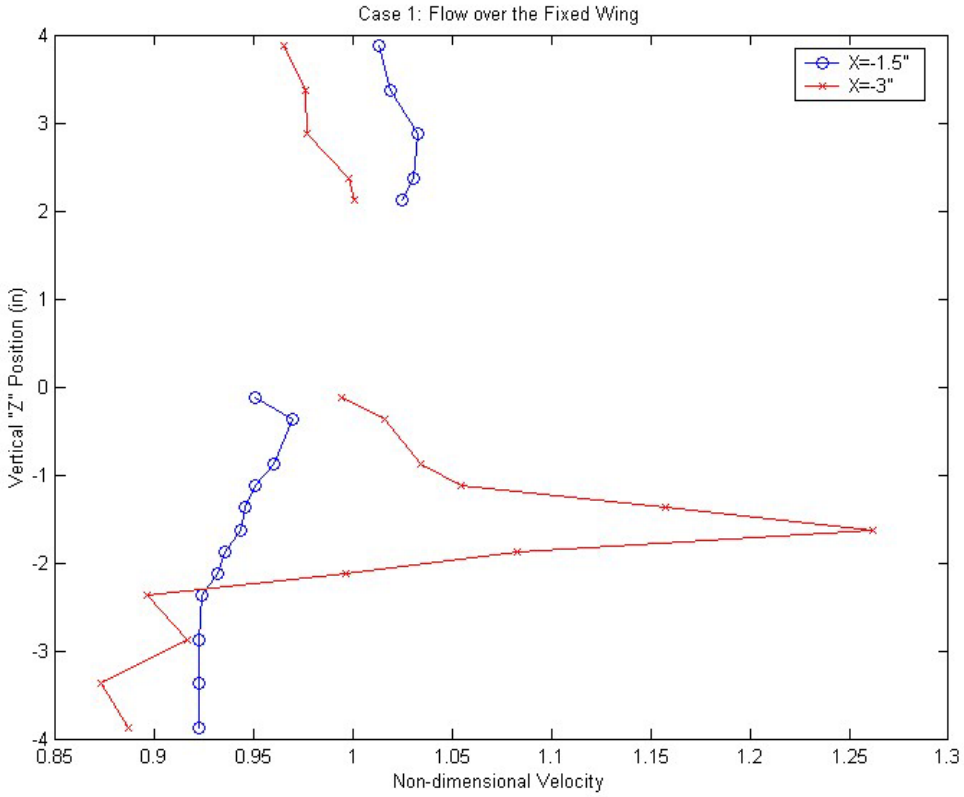

Figure 8. Flow over the Fixed Wing, Case 1

By way of contrast, Figure 9 illustrates the same model in the identical flight condition, except that the flapping wings are still and resting in their mean position. Note the sharp deceleration of the flow near the stagnation point of the flapping wing's (now stationary) leading edge.

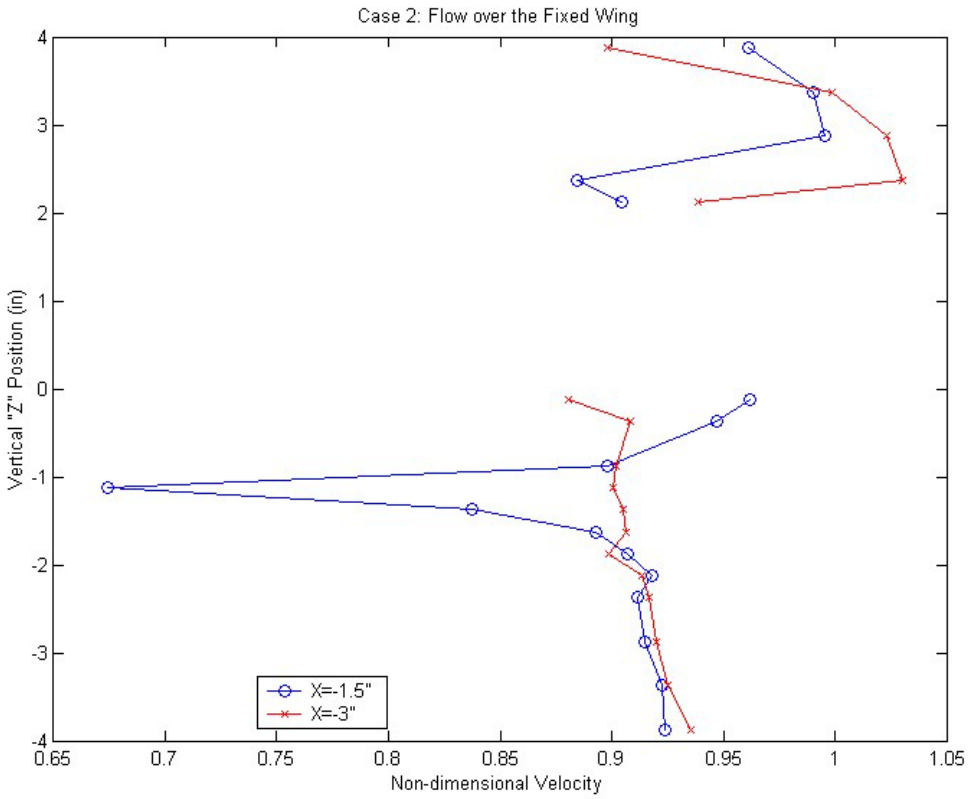

Figure 9. Flow over the Fixed Wing, Case 2

Figure 10 is an illustration of Case 3, in which the conditions are identical to Case 1, save for the absence of the fixed wing. The similarity of the plots indicates that the presence or absence of a fixed wing is no prerequisite for the entrainment of flow by the trailing flapping wings.

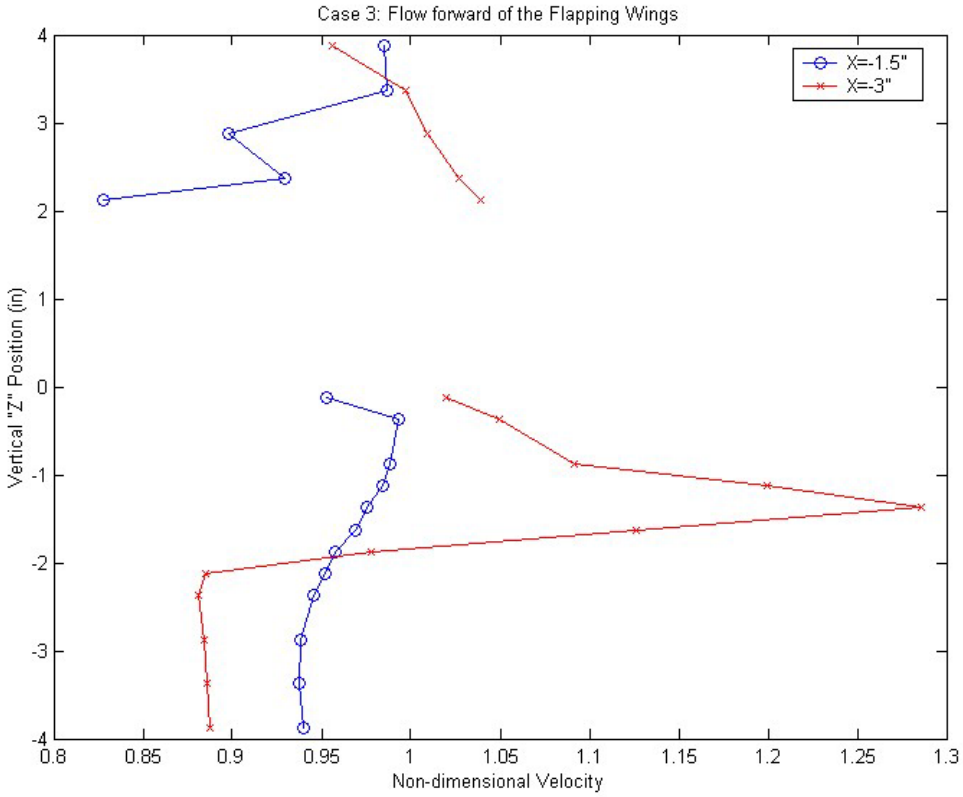

Figure 10. Flow forward of the Flapping Wings, Case 3

Figure 11 illustrates how much closer to the model's centerline the probe was able to approach in the absence of the fixed wing. With regard to the obvious asymmetry above and below, it may be speculated that this, too, is a reflection of the mean position of the flapping wing that is simply missed by the resolution on the upper surface and was only observed here by chance. It is the author's opinion that this merits further study.

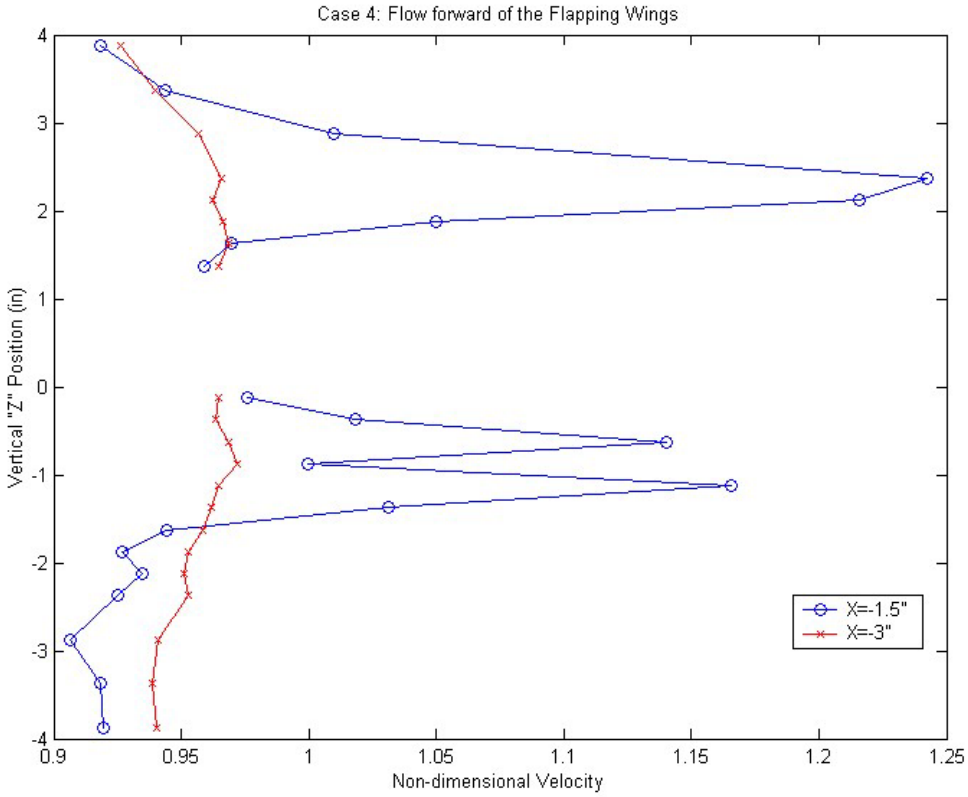

Figure 11. Flow forward of the Flapping Wings, Case 4

Case 5, in Figure 12 seems better able to illustrate the supposed symmetry of the flow above and below the wings, while Case 6, the with the fastest flapping rate of 38.4 Hz, seems again to have resolved a similar phenomenon, perhaps again by chance, and definitely again on the lower surface.

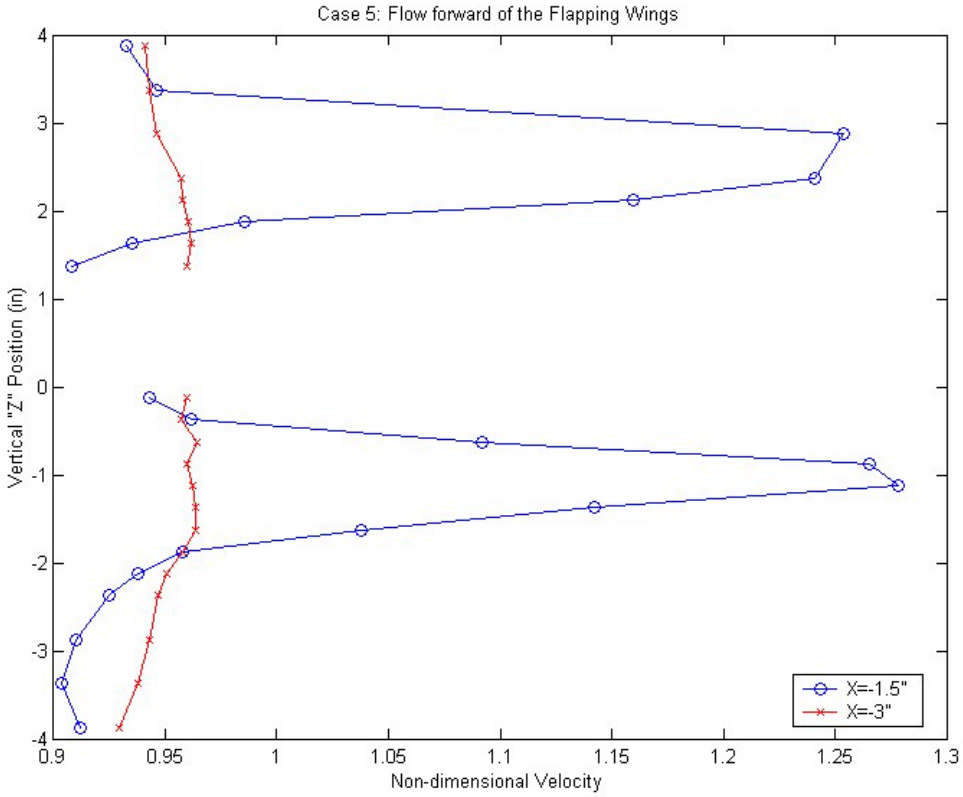

Figure 12. Flow forward of the Flapping Wings, Case 5

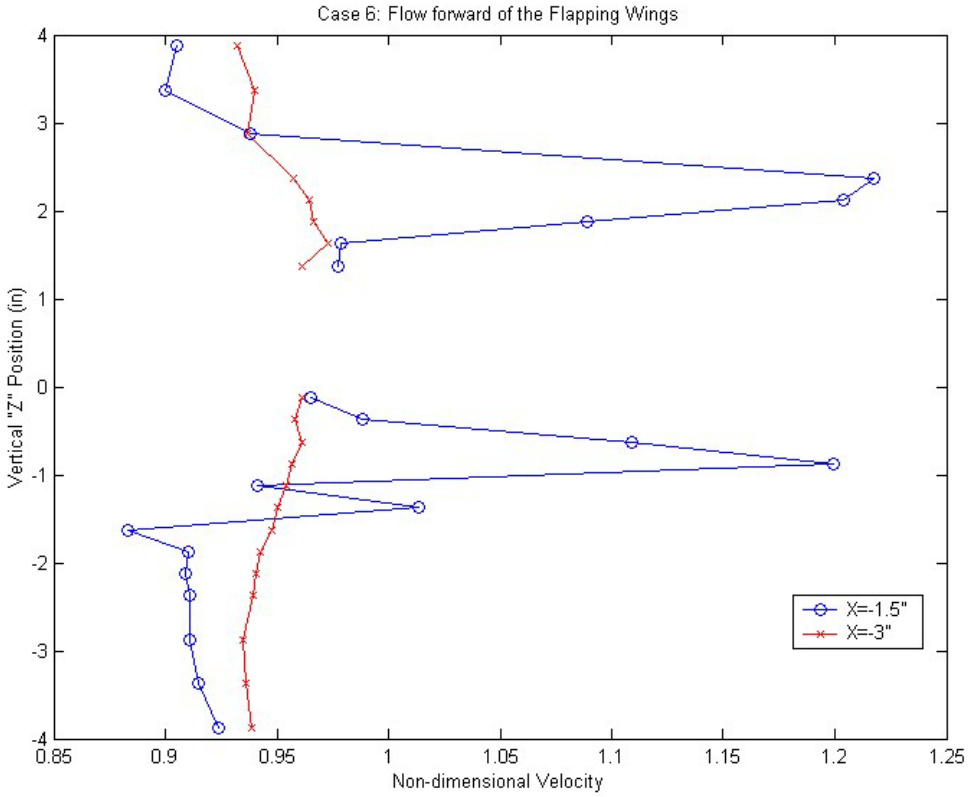

Figure 13. Flow forward of the Flapping Wings, Case 6

B. LDV VERSUS RMR MEAN VELOCITIES

When the LDV software, that is to say FIND® or PACE® solves for a mean velocity at a given locus in the flow field, it does so by means of averaging all of the velocities it measures there. This means that, if the flow is cyclical and if that cyclical flow allows more seed particles to pass through the probe volume at a certain part of the cycle than at other parts, the velocity will be weighted toward that of the heavier seeded part of the cycle.

Since the flow in the MAV's wake is heavily cyclical, it provides a distinct opportunity to study this condition.

In order to gather a non-weighted average, RMR data was taken. Now, the RMR will indeed collect more points during certain parts of the cycle than others, meaning that certain folders, each representing a five degree arc of the cycle, will be fuller than others. To counter this effect, each folder is quite simply weighted equally in what is referred to as the RMR mean velocity. This name is meant to distinguish it from the conventional LDV mean velocity, although, of course, both methods used the same LDV, and indeed, the same data; the only difference is in the weighting.

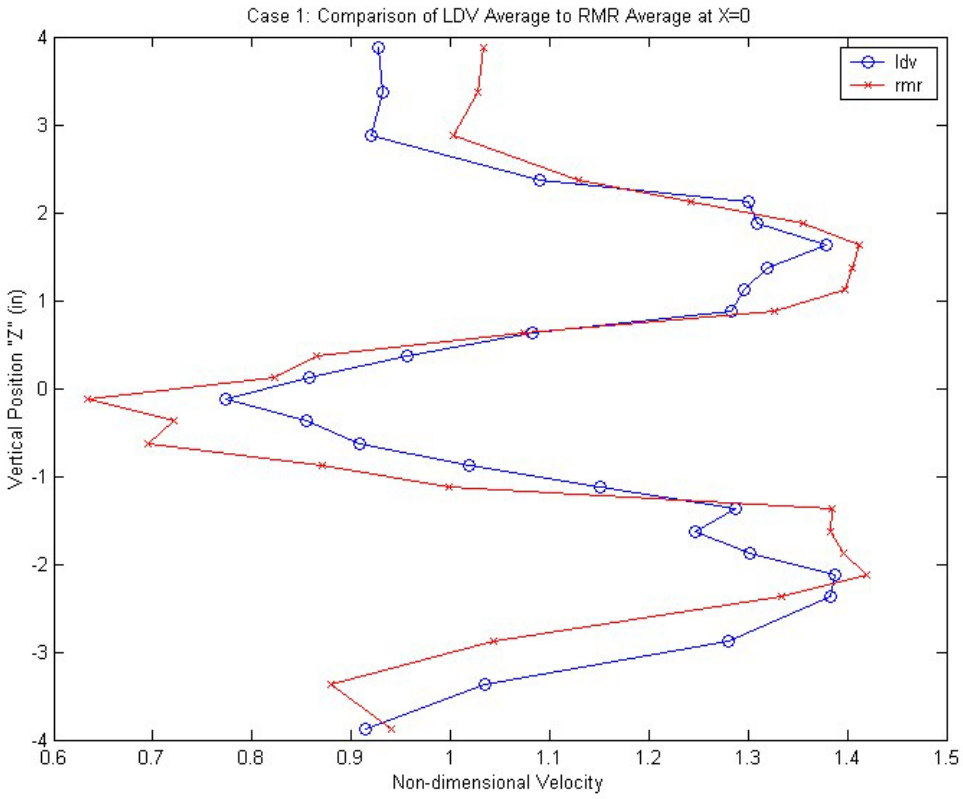

Figure 14. Comparison of LDV and RMR Average Velocities, Case 1 at X=0”

Figure 14 is fairly characteristic of the difference between LDV and RMR velocities. The two averages are generally similar within a few percent, but whether the LDV average will exaggerate the high speeds or low speeds or even tend to wash them out for the middle ground is rather unpredictable, since, as stated previously, it is heavily a function of seeding.

C. WAKE VARIATION OVER THE CYCLE

As one might expect, the velocity at a given point behind the flapping wing can vary considerably over the course of a 360° cycle. The following plots illustrate some of the variations in both the horizontal direction, where the mean is naturally positive, and the vertical direction where, in most cases, it averages to nearly zero.

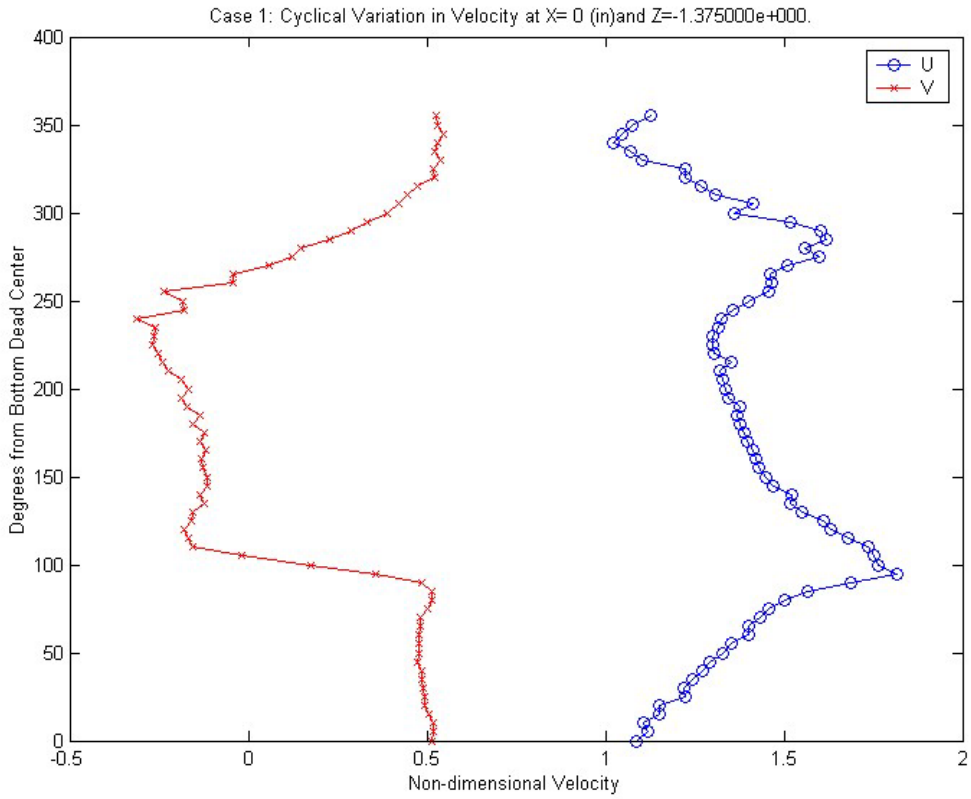

Figure 15. Cyclical Velocity Profile at X=0 & Z=-1.375

The example chosen here for discussion and shown in Figure 15 is particularly fascinating because it is at a point in space immediately aft of the lower flapping wing's trailing edge: a point that the trailing edge passes twice on each cycle, and a particularly well defined one at that. One can clearly see that the down-stroke creates a peak in the horizontal velocity as a jet of air is forced downstream. As well, the same passage, at about 100° from bottom-dead-center, generates two peaks in the vertical velocity component as the sign of the "V" velocity suddenly changes. Bottom-dead-center is perhaps more appropriate in reference to the upper flapping wing, but in any case it refers to the position in which the wings are as close

together as they can be, and BDC is used here as the reference position of 0°. It is especially interesting that these extrema appear so clearly even though the flapping wing is not pointed directly downstream. Indeed, the wing is inclined at 15° geometric angle of attack.

D. VELOCITY EXTREMES

In the interest of developing not only knowledge about the aerodynamics of flapping wing propulsion, but also developing a workable Micro Air Vehicle, one of the purposes of this study is to examine wind velocities near the model with an eye to finding a suitable location for control surfaces on the flying model. The best location will have relatively consistent flow. If there is too little airspeed the control surface will be ineffective, too much and the structural weight necessitated will ground the lightly built MAV. The plots shown below represent the minimum, mean, and maximum velocities measured at each location. For purposes of applicability, only the plots from Case 1 are shown, since they are most similar to actual flight conditions. The remainder may be viewed in the appendices.

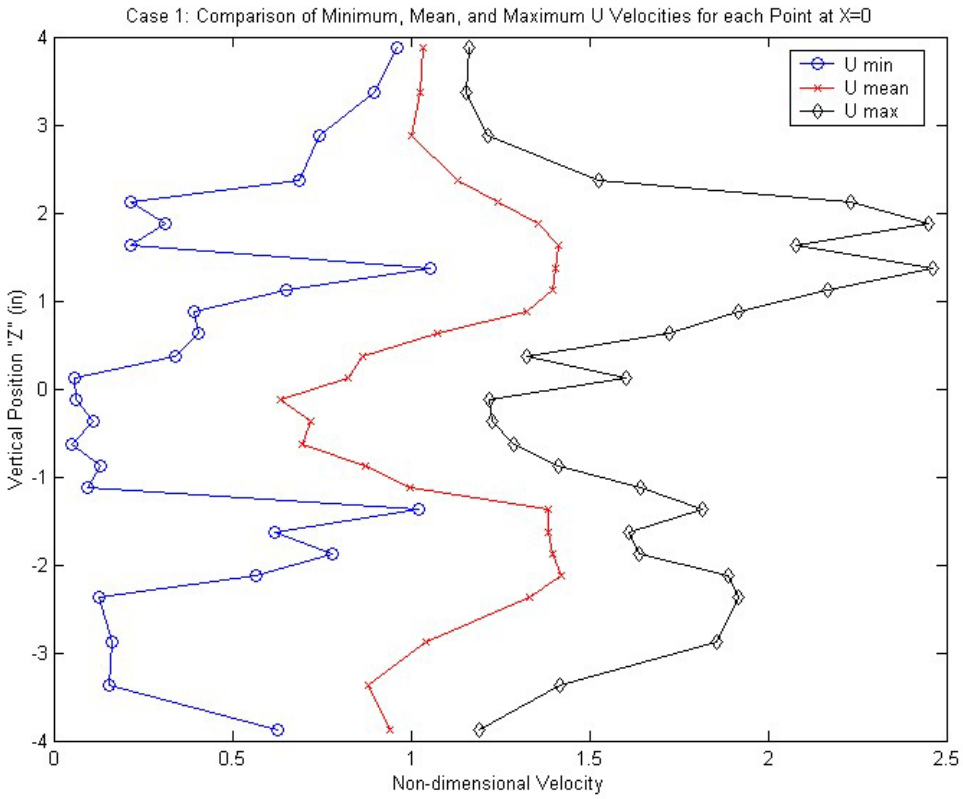

Figure 16. Minimum, Mean, and Maximum U Velocities at X=0, Case 1

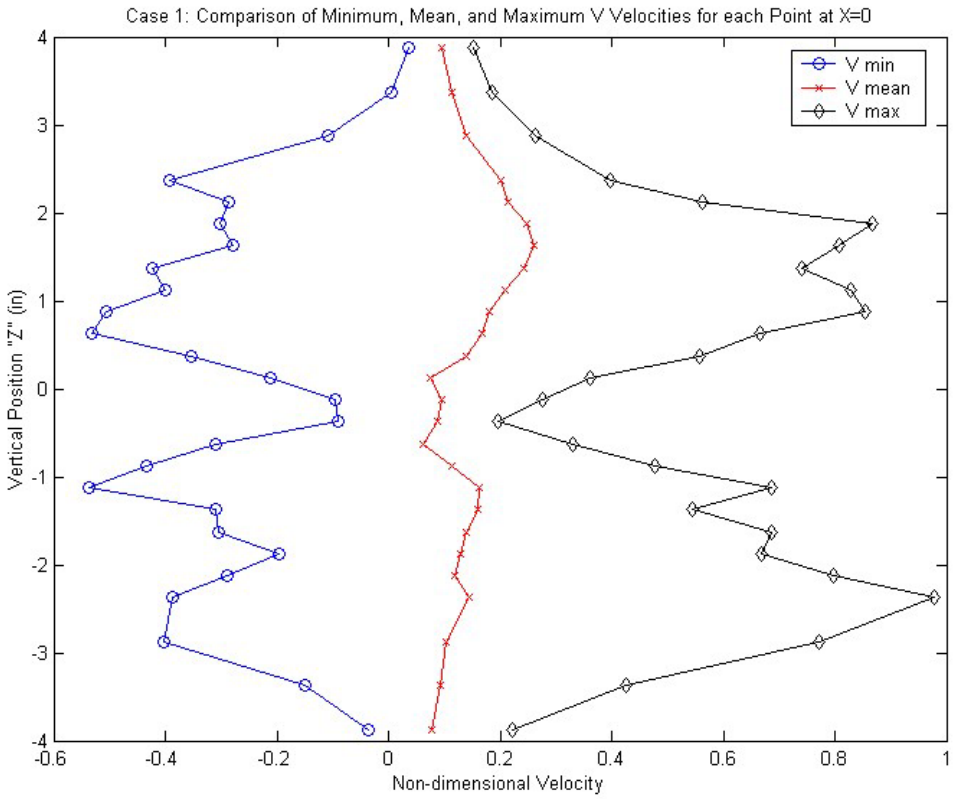

Figure 17. Minimum, Mean, and Maximum V Velocities at X=0, Case 1

E. WAKE DISSIPATION

Because a drag wake has a lower kinetic energy than the surrounding flow, it can be expected to be relatively more stable than a thrusting wake, which has a higher energy than the surrounding flow. This fact is demonstrated starkly in the figure below where both the thrusting and dragging wakes are extremely distinct at the X=0 position corresponding to the region immediately aft of the flapping wings' trailing edges. However, at the most downstream points, only 4.5" later, while the dragging wake a remains strong, the thrust wake is already dissipating into the freestream. In the current configuration, each flapping

wing generates its own thrusting wake. As these two wakes move downstream, they spread apart and become less distinct in the process. In the plots below, it will appear that the lower wake from Case 1 is descending while the upper one remains at a fairly constant height, and even to follow its brother slightly. The illusion is due to the sharp angle of attack at which the model is set. The wakes only move apart relative to the axis of the jet produced by the flapping. In this case, the jet is inclined at 15° relative to the axes of the LDV system.

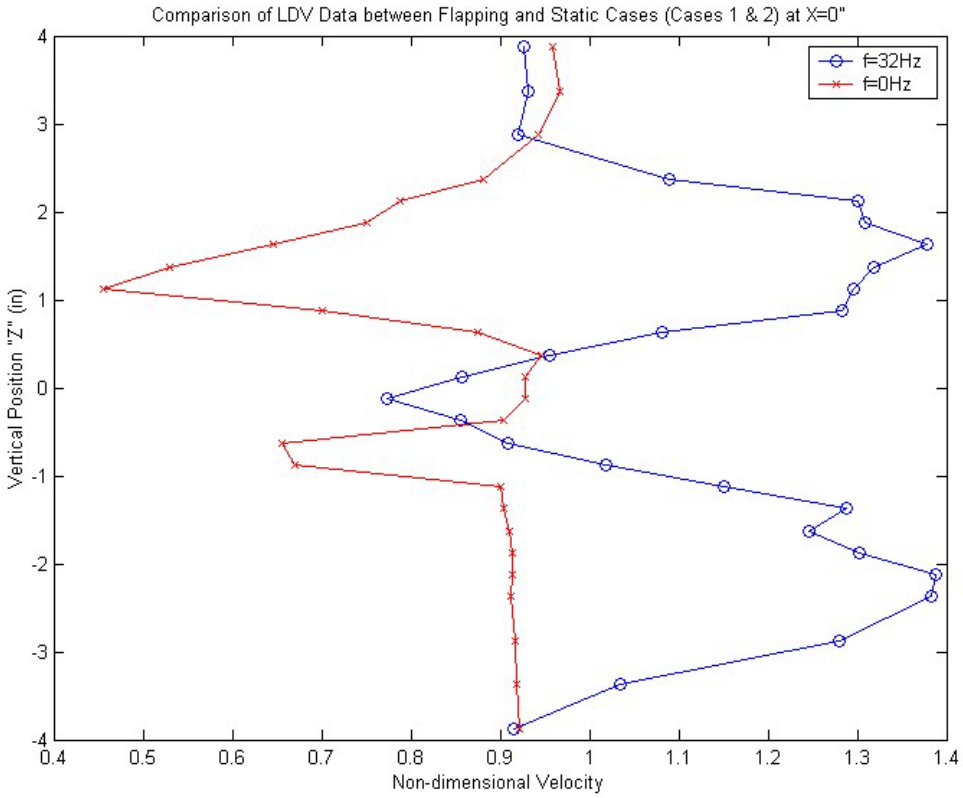

Figure 18. Streamwise Wake Profile Comparison at X=0, Cases 1 & 2

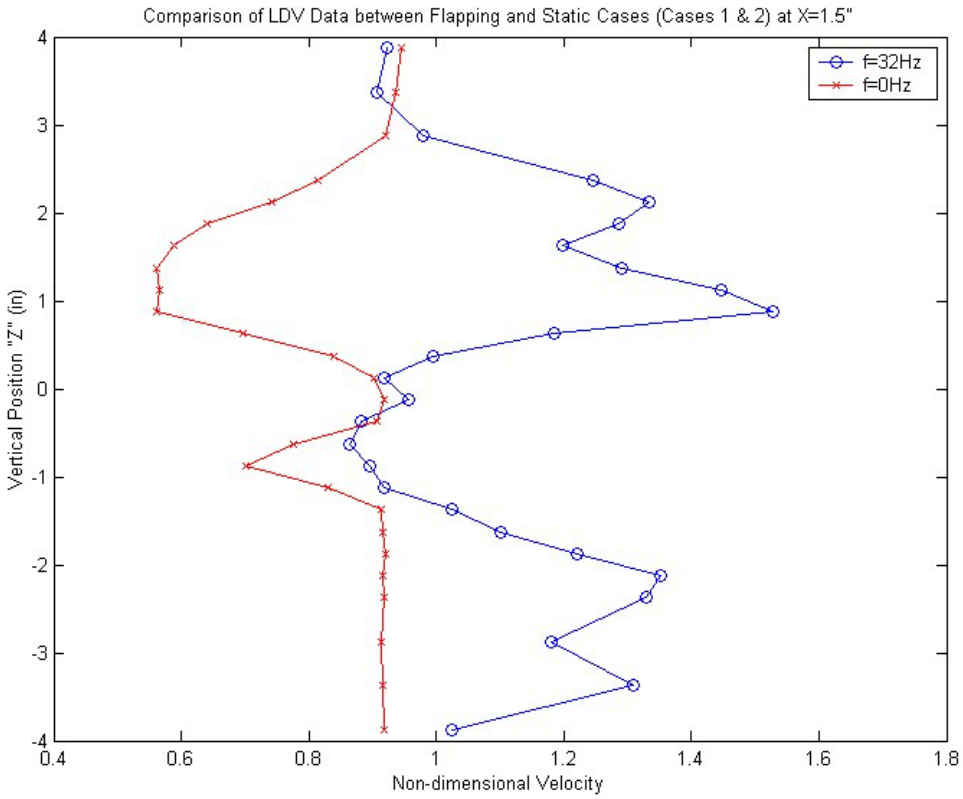

Figure 19. Streamwise Wake Profile Comparison at X=1.5”, Cases 1 & 2

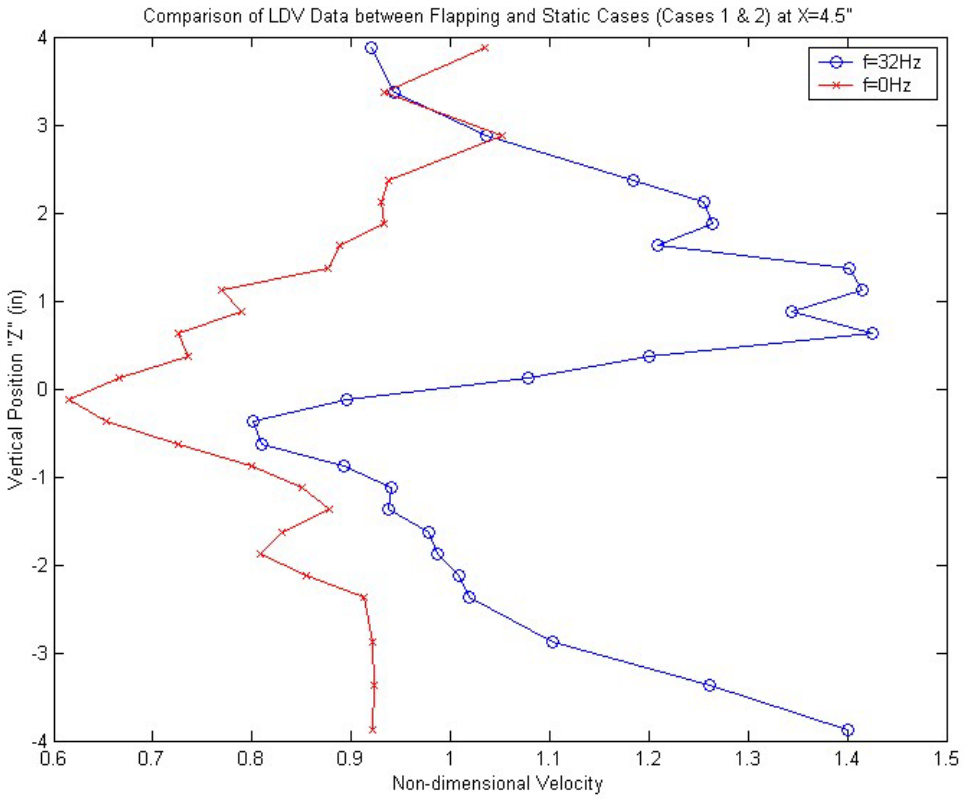

Figure 20. Streamwise Wake Profile Comparison at X=4.5”, Cases 1 & 2

V. CONCLUSIONS

With respect to each of the sub-headings in the results, a number of conclusions may be drawn.

Significant flow entrainment is apparent when the flapping wings are active. Indeed, examination of the wake profile of the static model at 15° angle of attack will reveal that the upper flapping wing is completely masked by the wake region of the fixed wing. Ergo, were it not for the entraining effects of the flapping wings, not only would the fixed wing be stalled, but also the upper flapping wing would be in such a separated flow condition that it would hardly be effective at all.

While conventional LDV velocity averages may be excellent for static cases, it pales in comparison to the RMR velocity average for a cyclical flow and should probably not be relied upon for more than a rough estimate in such a case.

Studies of wake variation over the cycle reveal that the wake velocity varies greatly across the regime. A more focused, more highly resolved analysis might reveal the answers to some of the new questions posed by the study here, especially with respect to the question about the leading edge stagnation point.

The plots of velocity extremes may be used to identify a potentially advantageous location for a control surface placement on the flying model. That decision will be left for the master MAV designer and builder, Prof. Kevin Jones, for consideration.

The thrust wake's spreading, as predicted by potential flow theory, is apparent in the wake profile plots; however, over the limited distance considered, it is difficult if not impossible to draw conclusions about the thrust wake's dissipation compared to that of the drag wake. In this respect, the physical dimensions of the traverse mechanism upon which the LDV probe rests impose a limitation.

APPENDIX A. MATLAB CODES

A. DATA FORMATTING

This code was used to get the .rmr files into a form usable by MATLAB. Each file was first imported as a matrix called "data," and then the code was run.

```
%load data into matrix, omitting empty W columns
combo=zeros(360,9);
combo(:,1)=data(:,2); %encoder position
combo(:,2)=data(:,3); %U pts
combo(:,3)=data(:,4); %V pts
combo(:,4)=3.28084*data(:,6); % U mean (fps)
combo(:,5)=3.28084*data(:,7); % V mean (fps)
combo(:,6)=data(:,9); % U std
combo(:,7)=data(:,10); % V std
combo(:,8)=data(:,12); % U TI%
combo(:,9)=data(:,13); % V TI %

%Compress 360 rows into 72 rows
mat=zeros(72,9);
for i=2:72;
    mat(i,:)=sum(combo([(5*i-6):(5*i-2)],:));
end
mat(1,:)=sum(combo([359,360,1,2,3],:));
```

```
mat(:,1)=[0:5:355]';
save c1_.xls mat -ascii -tabs
clear
```

B. PLOT GENERATION

This code was then run to generate the desired plots.

```
clear all

%initialize memory
a=zeros(5616,9);

%define indices
s=zeros(72,1);
e=s;
for i=1:78
    s(i)=72*(i-1)+1;
    e(i)=72*i;
end

%load data files into the matrix
i=1;
a(s(i):e(i),:)=load ('c1_1.xls');
i=i+1;
```

```
a(s(i):e(i),:)=load ('c1_2.xls');
i=i+1;
a(s(i):e(i),:)=load ('c1_3.xls');
i=i+1;
a(s(i):e(i),:)=load ('c1_4.xls');
i=i+1;
a(s(i):e(i),:)=load ('c1_5.xls');
i=i+1;
a(s(i):e(i),:)=load ('c1_6.xls');
i=i+1;
a(s(i):e(i),:)=load ('c1_7.xls');
i=i+1;
a(s(i):e(i),:)=load ('c1_8.xls');
i=i+1;
a(s(i):e(i),:)=load ('c1_9.xls');
i=i+1;
a(s(i):e(i),:)=load ('c1_10.xls');
i=i+1;
a(s(i):e(i),:)=load ('c1_11.xls');
i=i+1;
a(s(i):e(i),:)=load ('c1_12.xls');
i=i+1;
a(s(i):e(i),:)=load ('c1_13.xls');
i=i+1;
```

```
a(s(i):e(i),:)=load ('c1_14.xls');
i=i+1;
a(s(i):e(i),:)=load ('c1_15.xls');
i=i+1;
a(s(i):e(i),:)=load ('c1_16.xls');
i=i+1;
a(s(i):e(i),:)=load ('c1_17.xls');
i=i+1;
a(s(i):e(i),:)=load ('c1_18.xls');
i=i+1;
a(s(i):e(i),:)=load ('c1_19.xls');
i=i+1;
a(s(i):e(i),:)=load ('c1_20.xls');
i=i+1;
a(s(i):e(i),:)=load ('c1_21.xls');
i=i+1;
a(s(i):e(i),:)=load ('c1_22.xls');
i=i+1;
a(s(i):e(i),:)=load ('c1_23.xls');
i=i+1;
a(s(i):e(i),:)=load ('c1_24.xls');
i=i+1;
a(s(i):e(i),:)=load ('c1_25.xls');
i=i+1;
```

```
a(s(i):e(i),:)=load ('c1_26.xls');
i=i+1;
a(s(i):e(i),:)=load ('c1_27.xls');
i=i+1;
a(s(i):e(i),:)=load ('c1_28.xls');
i=i+1;
a(s(i):e(i),:)=load ('c1_29.xls');
i=i+1;
a(s(i):e(i),:)=load ('c1_30.xls');
i=i+1;
a(s(i):e(i),:)=load ('c1_31.xls');
i=i+1;
a(s(i):e(i),:)=load ('c1_32.xls');
i=i+1;
a(s(i):e(i),:)=load ('c1_33.xls');
i=i+1;
a(s(i):e(i),:)=load ('c1_34.xls');
i=i+1;
a(s(i):e(i),:)=load ('c1_35.xls');
i=i+1;
a(s(i):e(i),:)=load ('c1_36.xls');
i=i+1;
a(s(i):e(i),:)=load ('c1_37.xls');
i=i+1;
```

```
a(s(i):e(i),:)=load ('c1_38.xls');
i=i+1;
a(s(i):e(i),:)=load ('c1_39.xls');
i=i+1;
a(s(i):e(i),:)=load ('c1_40.xls');
i=i+1;
a(s(i):e(i),:)=load ('c1_41.xls');
i=i+1;
a(s(i):e(i),:)=load ('c1_42.xls');
i=i+1;
a(s(i):e(i),:)=load ('c1_43.xls');
i=i+1;
a(s(i):e(i),:)=load ('c1_44.xls');
i=i+1;
a(s(i):e(i),:)=load ('c1_45.xls');
i=i+1;
a(s(i):e(i),:)=load ('c1_46.xls');
i=i+1;
a(s(i):e(i),:)=load ('c1_47.xls');
i=i+1;
a(s(i):e(i),:)=load ('c1_48.xls');
i=i+1;
a(s(i):e(i),:)=load ('c1_49.xls');
i=i+1;
```

```
a(s(i):e(i),:)=load ('c1_50.xls');
i=i+1;
a(s(i):e(i),:)=load ('c1_51.xls');
i=i+1;
a(s(i):e(i),:)=load ('c1_52.xls');
i=i+1;
a(s(i):e(i),:)=load ('c1_53.xls');
i=i+1;
a(s(i):e(i),:)=load ('c1_54.xls');
i=i+1;
a(s(i):e(i),:)=load ('c1_55.xls');
i=i+1;
a(s(i):e(i),:)=load ('c1_56.xls');
i=i+1;
a(s(i):e(i),:)=load ('c1_57.xls');
i=i+1;
a(s(i):e(i),:)=load ('c1_58.xls');
i=i+1;
a(s(i):e(i),:)=load ('c1_59.xls');
i=i+1;
a(s(i):e(i),:)=load ('c1_60.xls');
i=i+1;
a(s(i):e(i),:)=load ('c1_61.xls');
i=i+1;
```

```
a(s(i):e(i),:)=load ('c1_62.xls');
i=i+1;
a(s(i):e(i),:)=load ('c1_63.xls');
i=i+1;
a(s(i):e(i),:)=load ('c1_64.xls');
i=i+1;
a(s(i):e(i),:)=load ('c1_65.xls');
i=i+1;
a(s(i):e(i),:)=load ('c1_66.xls');
i=i+1;
a(s(i):e(i),:)=load ('c1_67.xls');
i=i+1;
a(s(i):e(i),:)=load ('c1_68.xls');
i=i+1;
a(s(i):e(i),:)=load ('c1_69.xls');
i=i+1;
a(s(i):e(i),:)=load ('c1_70.xls');
i=i+1;
a(s(i):e(i),:)=load ('c1_71.xls');
i=i+1;
a(s(i):e(i),:)=load ('c1_72.xls');
i=i+1;
a(s(i):e(i),:)=load ('c1_73.xls');
i=i+1;
```

```
a(s(i):e(i),:)=load ('c1_74.xls');
i=i+1;
a(s(i):e(i),:)=load ('c1_75.xls');
i=i+1;
a(s(i):e(i),:)=load ('c1_76.xls');
i=i+1;
a(s(i):e(i),:)=load ('c1_77.xls');
i=i+1;
a(s(i):e(i),:)=load ('c1_78.xls');
i=i+1;
ldv=xlsread('Case1.xls');

%inspect matrices to be sure they are properly
%built by being certain that columns are not repeated

%Compare matrix to itself
for i=(1:78)
    if a(s(i),4)==a(s(i),5)
        disp ('rebuild matrix number')
        disp(i)
    end
end
%Compare matrices to each other
for i=(2:78)
```

```
    if a(s(i),4)==a(s(i-1),4)
        disp ('rebuild matrix number', i)
    elseif a(s(i),5)==a(s(i-1),5)
        disp ('rebuild matrix number', i)
    end
end

%Ensure minimum number of points in each file
minupts=min(a(1:5616,2))
minvpts=min(a(1:5616,3))

%Normalize data
Vinf=9.1864 %fps
a(:,4)=a(:,4)/Vinf; % U mean
a(:,5)=a(:,5)/Vinf; % V mean

%plots
zcoords=[3.875  ;3.375;  2.875  ;2.375;  2.125  ;1.875
;1.625 ;1.375; 1.125 ;0.875 ;0.625; 0.375 ;0.125;
-0.125; -0.375; -0.625 ;-0.875 ;-1.125; -1.375; -1.625
;-1.875 ;-2.125; -2.375; -2.875 ;-3.375 ;-3.875];
```

```
%non-point weighted average
for i=1:78
rmr(i,:)=mean(a(s(i):(e(i)),:));
Uavg(i,1)=mean(a(s(i):(e(i)),4));
Vavg(i,1)=mean(a(s(i):(e(i)),5));
end
fig=1;
figure(fig)
plot(Uavg(1:26,1),zcoords,'bo-')
hold on
plot(Uavg(27:52,1),zcoords,'rx-')
hold on
plot(Uavg(53:78,1),zcoords,'kd-')
title('Case 1: Wake Profile, RMR')
ylabel('Vertical Position "Z" (in)')
xlabel('Non-dimensional Velocity')
legend
legend('x=0','x=1.5"','x=4.5"')



%Comparison to point weighted average
fig=fig+1;
figure(fig)
```

```
     plot(ldv(1:26,5)/Vinf,zcoords,'bo-',
Uavg(1:26),zcoords,'rx-')
     legend('ldv','rmr')
     title('Case 1: Comparison of LDV Average to RMR
Average at X=0')
     ylabel('Vertical Position "Z" (in)')
     xlabel('Non-dimensional Velocity')

     fig=fig+1;
     figure(fig)
     plot(ldv(27:52,5)/Vinf,zcoords,'bo-',
Uavg(27:52),zcoords,'rx-')
     legend('ldv','rmr')
     title('Case 1: Comparison of LDV Average to RMR
Average at X=1.5"')
     ylabel('Vertical Position "Z" (in)')
     xlabel('Non-dimensional Velocity')

     fig=fig+1;
     figure(fig)
     plot(ldv(53:78,5)/Vinf,zcoords,'bo-',
Uavg(53:78),zcoords,'rx-')
     legend('ldv','rmr')
     title('Case 1: Comparison of LDV Average to RMR
Average at X=4.5"')
```

```
ylabel('Vertical Position "Z" (in)')
xlabel('Non-dimensional Velocity')


Umin=zeros(78,1);
Vmin=zeros(78,1);
for i=1:78
Umin(i,1)=min(a(s(i):e(i),4));
Vmin(i,1)=min(a(s(i):e(i),5));
Umax(i,1)=max(a(s(i):e(i),4));
Vmax(i,1)=max(a(s(i):e(i),5));
end
fig=fig+1;
figure(fig)
plot(Umin(1:26),zcoords,'bo-',  Uavg(1:26),zcoords,'rx-
',Umax(1:26),zcoords,'kd-')
legend('U min','U mean', 'U max',0)
title('Case  1:  Comparison  of  Minimum,  Mean,  and
Maximum U Velocities for each Point at X=0')
ylabel('Vertical Position "Z" (in)')
xlabel('Non-dimensional Velocity')

fig=fig+1;
figure(fig)
```

```
plot(Umin(27:52),zcoords,'bo-',
Uavg(27:52),zcoords,'rx-',Umax(27:52),zcoords,'kd-')
legend('U min','U mean', 'U max',0)
title('Case 1: Comparison of Minimum, Mean, and
Maximum U Velocities for each Point at X=1.5"')
ylabel('Vertical Position "Z" (in)')
xlabel('Non-dimensional Velocity')

fig=fig+1;
figure(fig)
plot(Umin(53:78),zcoords,'bo-',
Uavg(53:78),zcoords,'rx-',Umax(53:78),zcoords,'kd-')
legend('U min','U mean', 'U max',0)
title('Case 1: Comparison of Minimum, Mean, and
Maximum U Velocities for each Point at X=4.5"')
ylabel('Vertical Position "Z" (in)')
xlabel('Non-dimensional Velocity')

fig=fig+1;
figure(fig)
plot(Vmin(1:26),zcoords,'bo-', Vavg(1:26),zcoords,'rx-
',Vmax(1:26),zcoords,'kd-')
legend('V min','V mean', 'V max',0)
title('Case 1: Comparison of Minimum, Mean, and
Maximum V Velocities for each Point at X=0')
```

```
ylabel('Vertical Position "Z" (in)')
xlabel('Non-dimensional Velocity')

fig=fig+1;
figure(fig)
plot(Vmin(27:52),zcoords,'bo-',
Vavg(27:52),zcoords,'rx-',Vmax(27:52),zcoords,'kd-')
legend('V min','V mean', 'V max',0)
title('Case 1: Comparison of Minimum, Mean, and
Maximum V Velocities for each Point at X=1.5"')
ylabel('Vertical Position "Z" (in)')
xlabel('Non-dimensional Velocity')

fig=fig+1;
figure(fig)
plot(Vmin(53:78),zcoords,'bo-',
Vavg(53:78),zcoords,'rx-',Vmax(53:78),zcoords,'kd-')
legend('V min','V mean', 'V max',0)
title('Case 1: Comparison of Minimum, Mean, and
Maximum V Velocities for each Point at X=4.5"')
ylabel('Vertical Position "Z" (in)')
xlabel('Non-dimensional Velocity')

zpos=[zcoords;zcoords;zcoords];
```

```
for i=1:78
    %define x location
    xpos=1.5;
    if i<27
        xpos=0;
    elseif i>52
        xpos=4.5;
    end
fig=fig+1;
figure(fig);
plot(a(s(i):e(i),4),a(s(i):e(i),1),'bo-') %U
hold on
plot(a(s(i):e(i),5),a(s(i):e(i),1),'rx-') %V
legend('U','V',0)
z=zpos(i,1);
string=sprintf('Case 1: Cyclical Variation in Velocity
at X= %d (in)and Z=%d. %d (in)%d.', xpos, z);
title(string)
ylabel('Degrees from Bottom Dead Center')
xlabel('Non-dimensional Velocity')
end
```

```
%Save the plots to file
for i=1:fig
    if i>10
        fname=sprintf('C1pt%d.jpg%d.',i-10);
    elseif i==1
        fname=sprintf('C1wakpro.jpg');
    elseif i==2
        fname=sprintf('C1lr0.jpg');
    elseif i==3
        fname=sprintf('C1lr15.jpg');
    elseif i==4
        fname=sprintf('C1lr45.jpg');
    elseif i==5
        fname=sprintf('C1Ummm0');
    elseif i==6
        fname=sprintf('C1Ummm15.jpg');
    elseif i==7
        fname=sprintf('C1Ummm45.jpg');
    elseif i==8
        fname=sprintf('C1Vmmm0.jpg');
    elseif i==9
        fname=sprintf('C1Vmmm15.jpg');
    elseif i==10
        fname=sprintf('C1Vmmm45.jpg');
```

```
    end
    print(figure(i),'-djpeg90','-r100',fname)
end

%Save data to files
for i=1:78
    ptmat=a(s(i):e(i),:);
    fname=sprintf('C1pt%d.xls%d.',i);
    save (fname, 'ptmat','-ascii','-tabs')
end
disp('Done.')
```

APPENDIX B. PLOTS FROM CASE 1

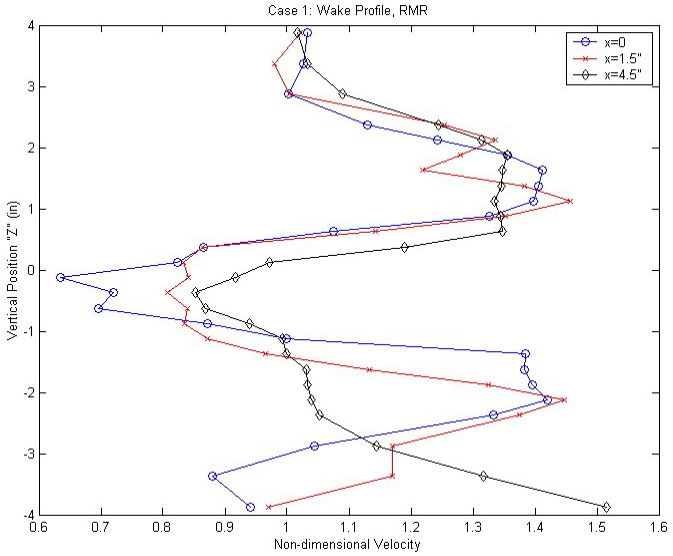

Figure 21. Wake Profiles for Case 1

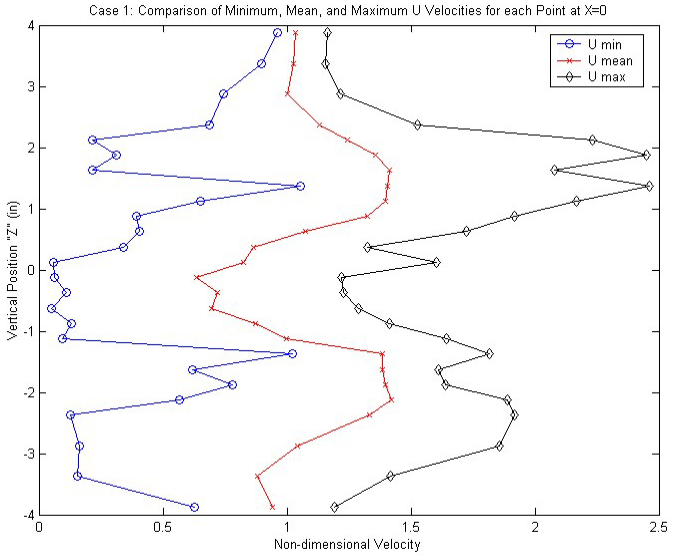

Figure 22. Minimum, Mean, and Maximum U Velocities for X=0, Case 1

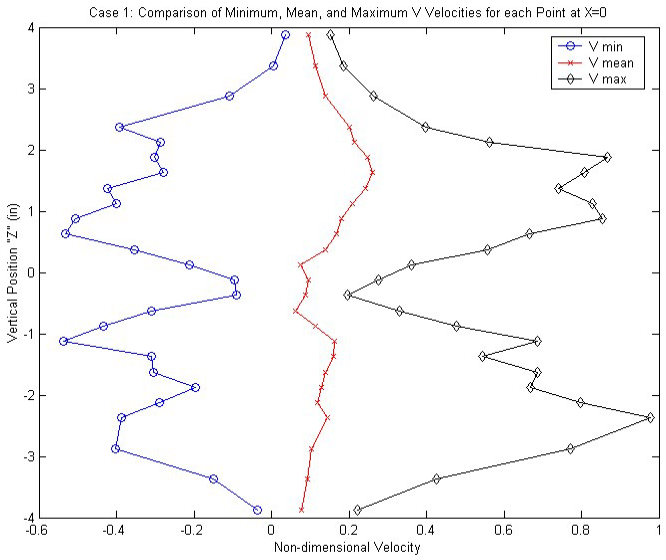

Figure 23. Minimum, Mean, and Maximum V Velocities for X=0, Case 1

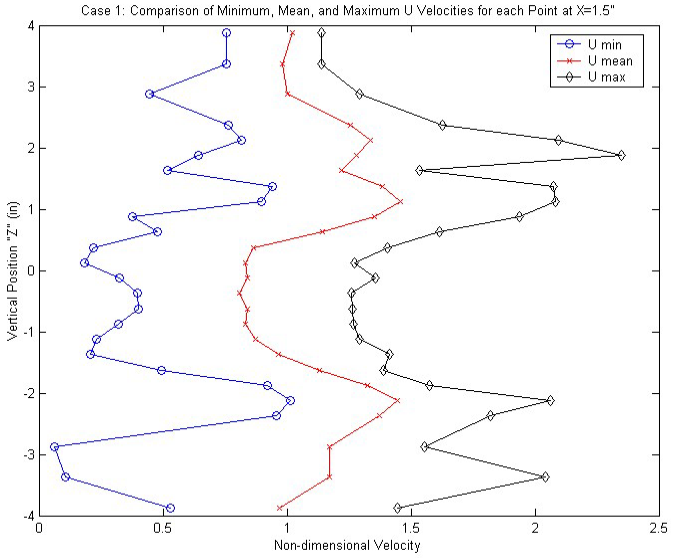

Figure 24. Minimum, Mean, and Maximum U Velocities for X=1.5”, Case 1

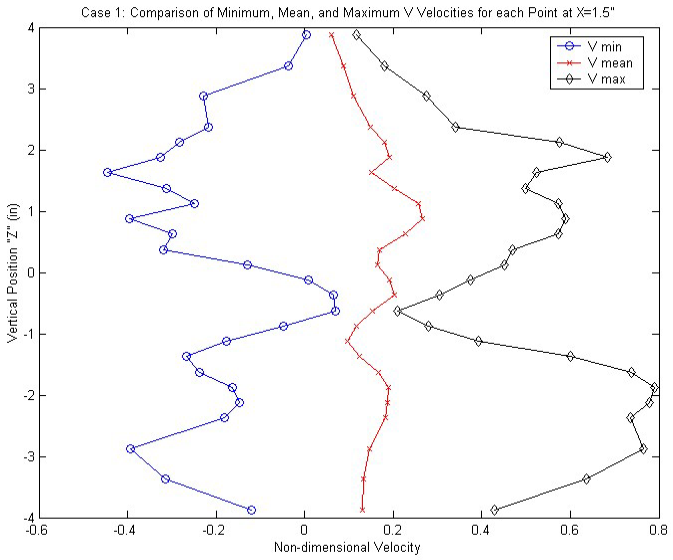

Figure 25. Minimum, Mean, and Maximum V Velocities for X=1.5”, Case 1

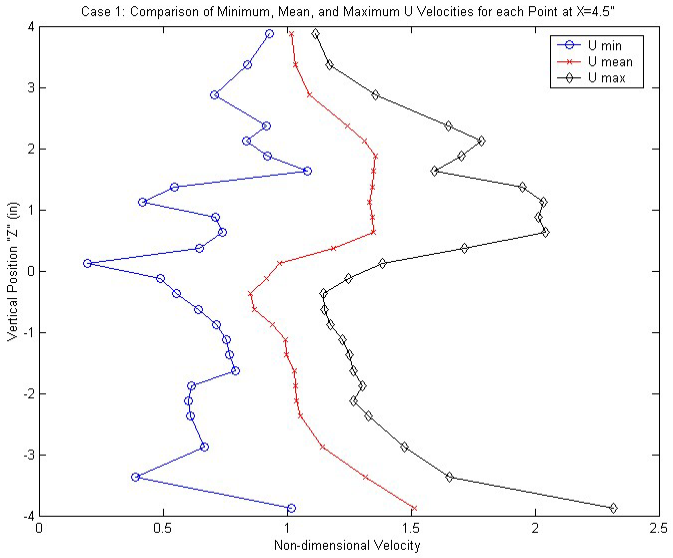

Figure 26. Minimum, Mean, and Maximum U Velocities for X=4.5”, Case 1

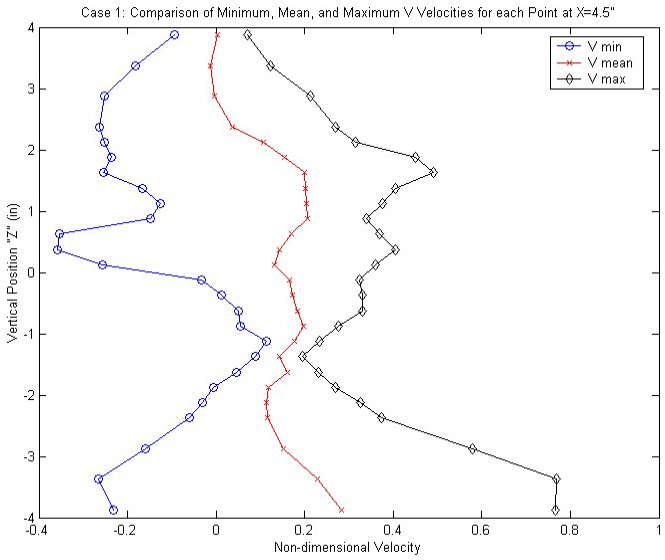

Figure 27. Minimum, Mean, and Maximum V Velocities for X=4.5”, Case 1

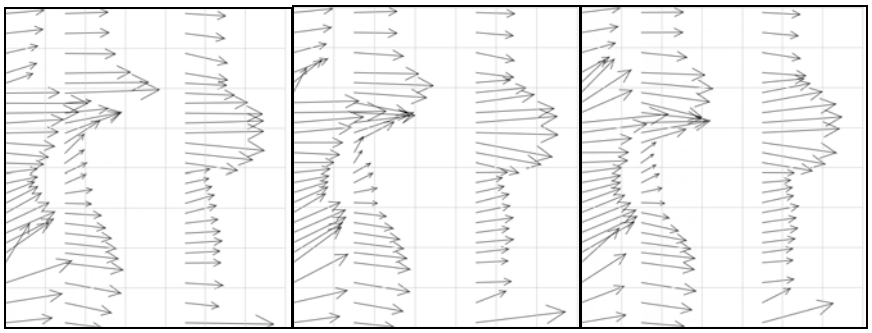

ϕ=0 ϕ=15 ϕ=30

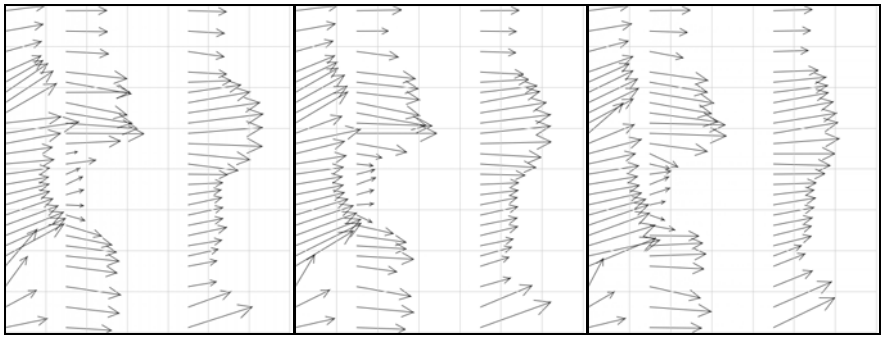

ϕ=45 ϕ=60 ϕ=75

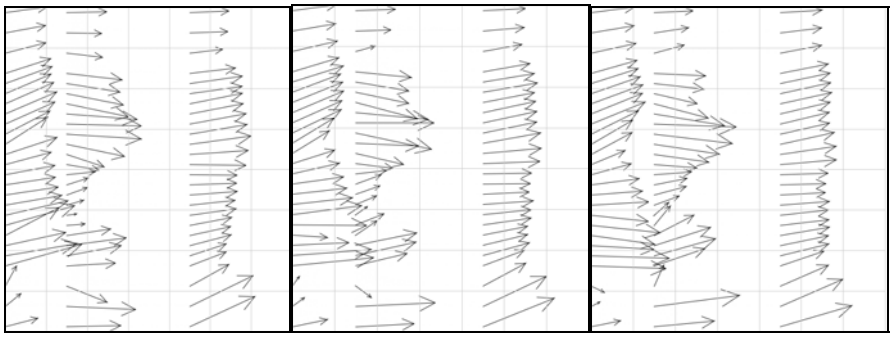

ϕ=90 ϕ=105 ϕ=120

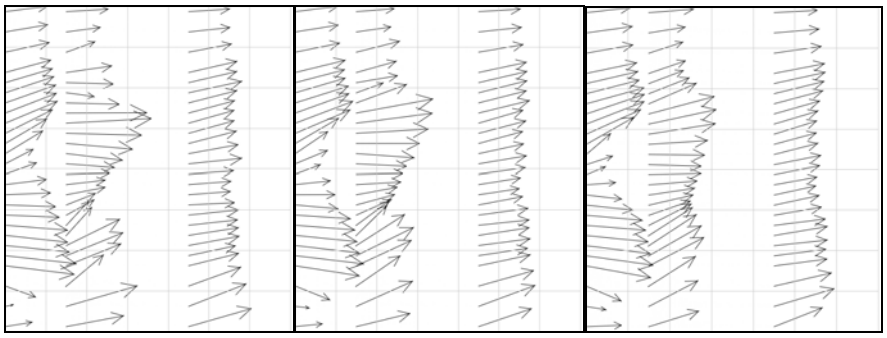

ϕ=135 ϕ=150 ϕ=165

Figure 28. Case 1 Wake Profiles, 0-165°

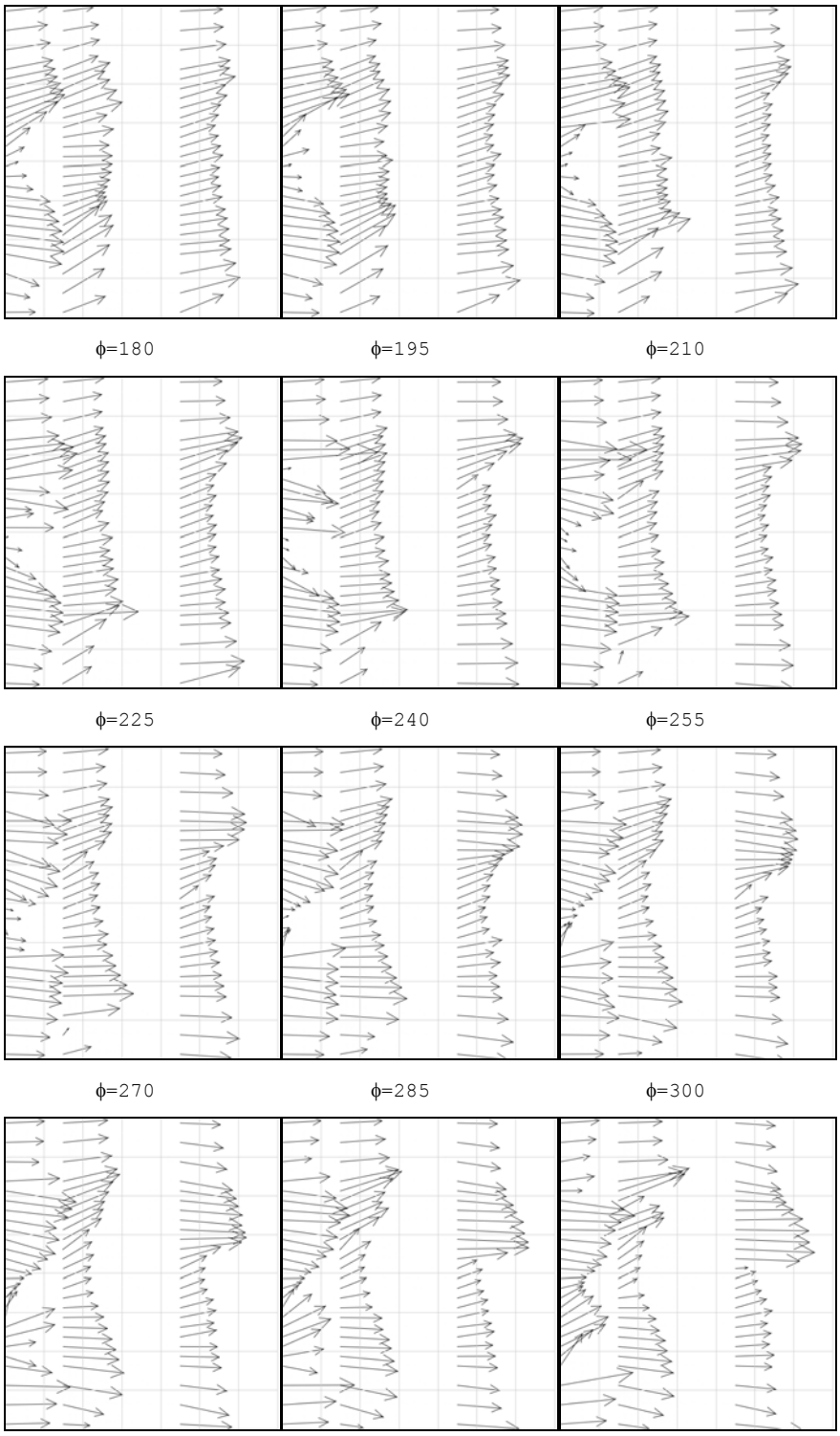

Figure 29. Case 1 Wake Profiles, 180-345°

APPENDIX C. DATA FROM CASE 2

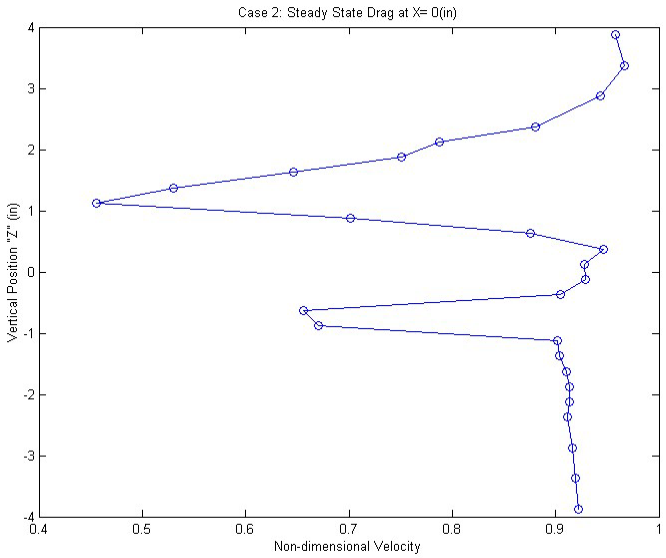

Figure 30. Drag Wake Profile at X=0

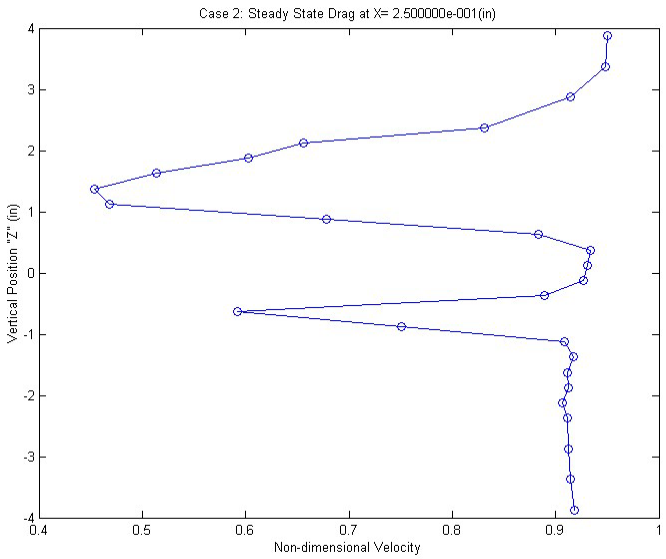

Figure 31. Drag Wake Profile at X=0.25”

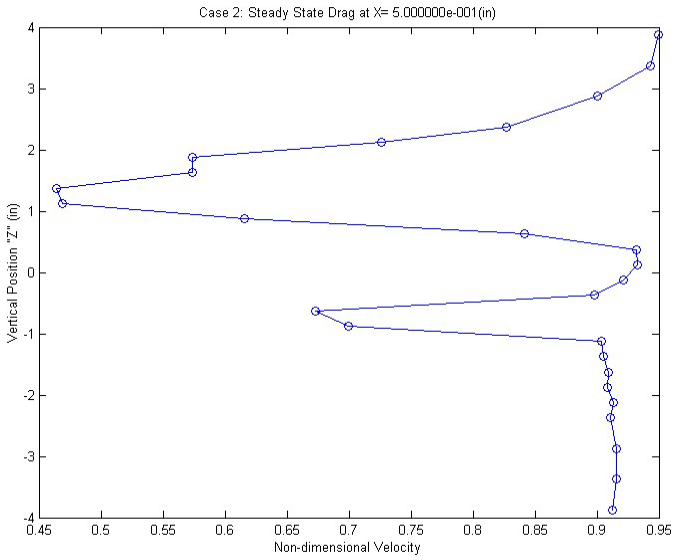

Figure 32. Drag Wake Profile at X=0.5”

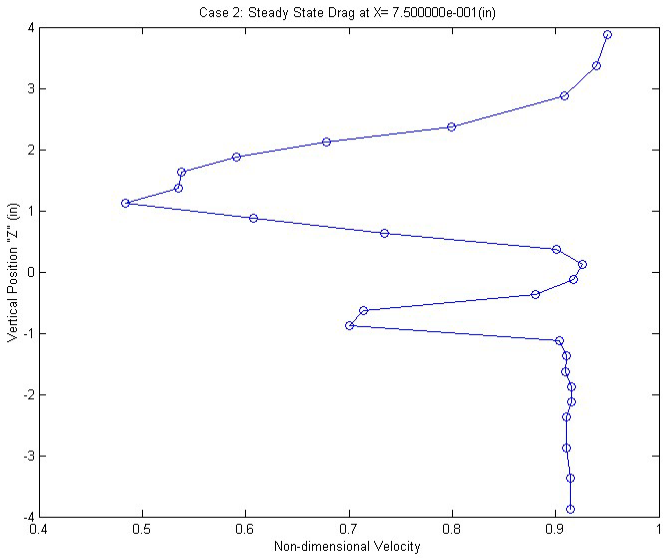

Figure 33. Drag Wake Profile at X=0.75”

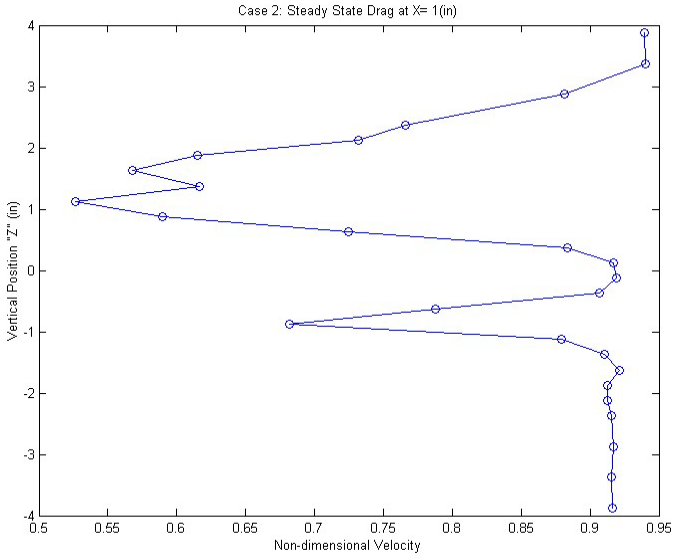

Figure 34. Drag Wake Profile at X=1”

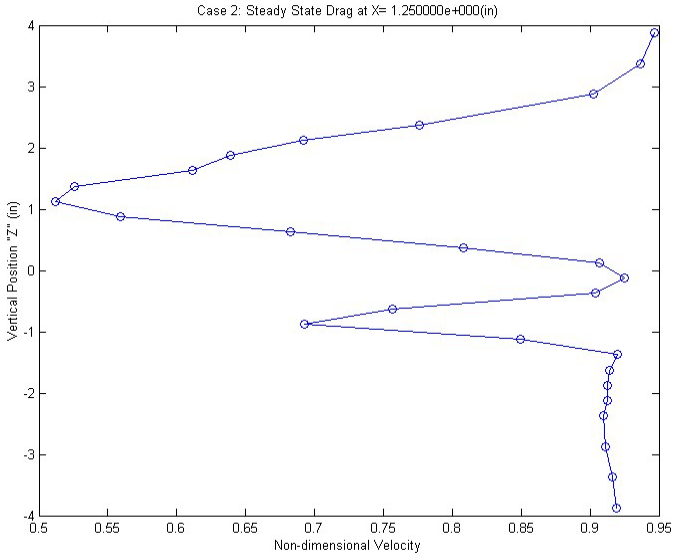

Figure 35. Drag Wake Profile at X=1.25”

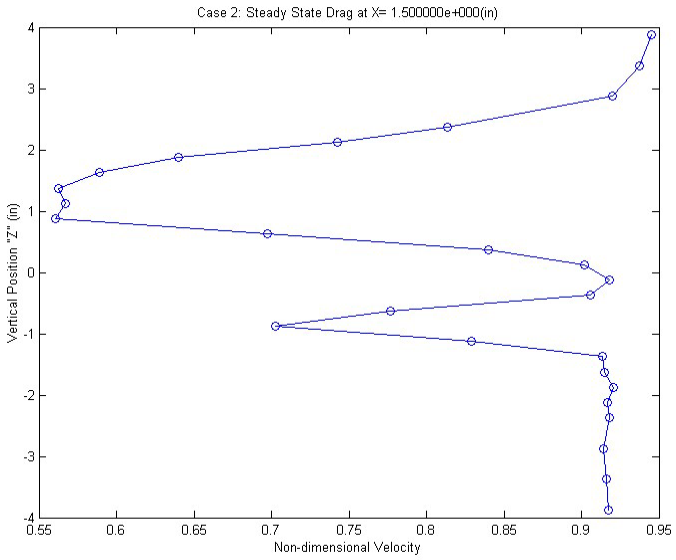

Figure 36. Drag Wake Profile at X=1.5”

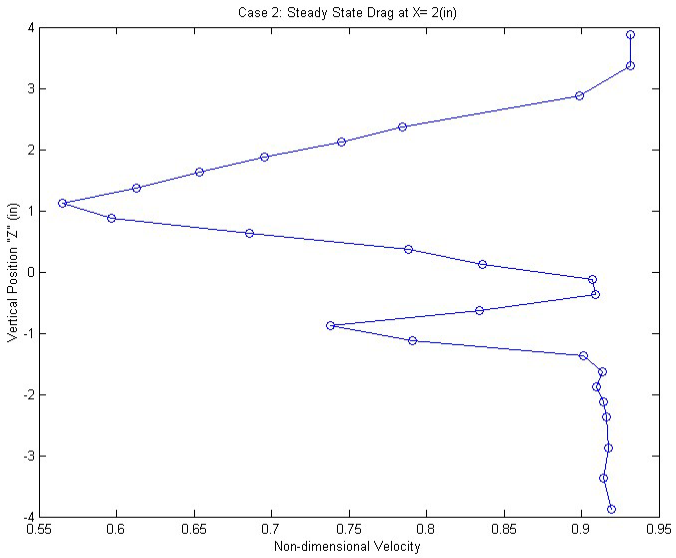

Figure 37. Drag Wake Profile at X=2”

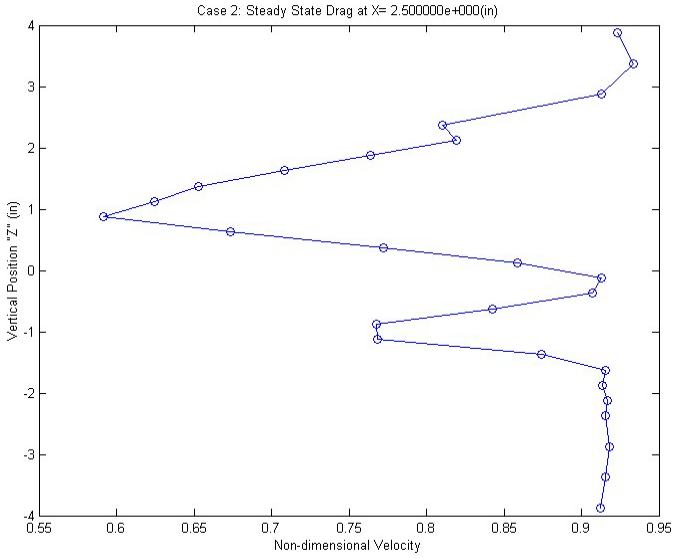

Figure 38. Drag Wake Profile at X=2.5”

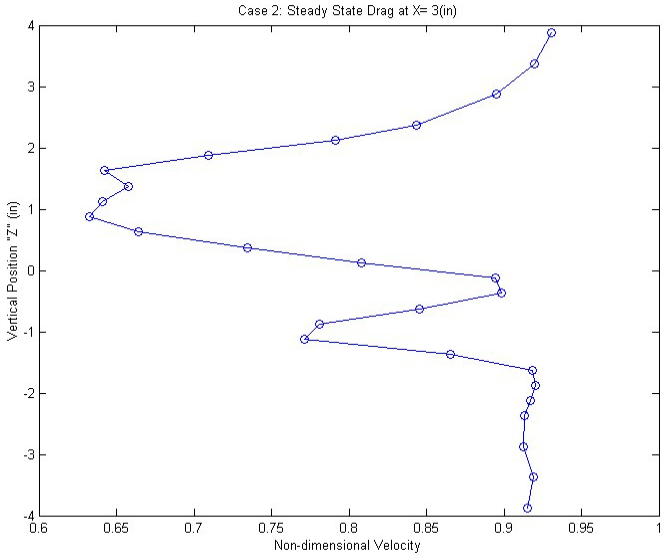

Figure 39. Drag Wake Profile at X=3”

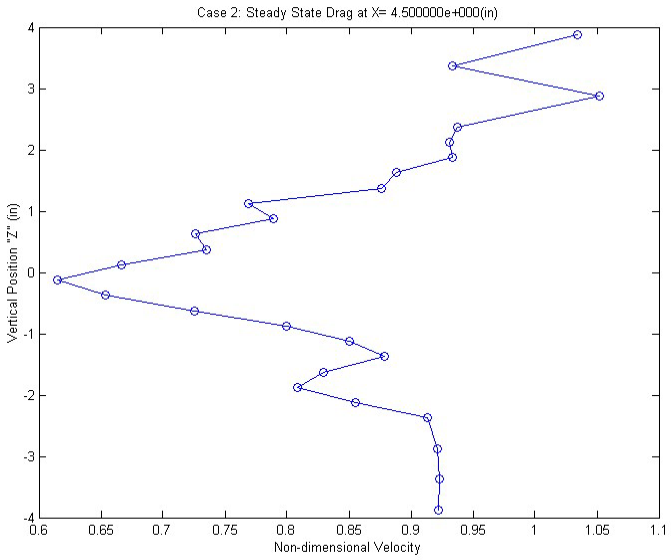

Figure 40. Drag Wake Profile at X=4.5”

APPENDIX D. PLOTS FROM CASE 3

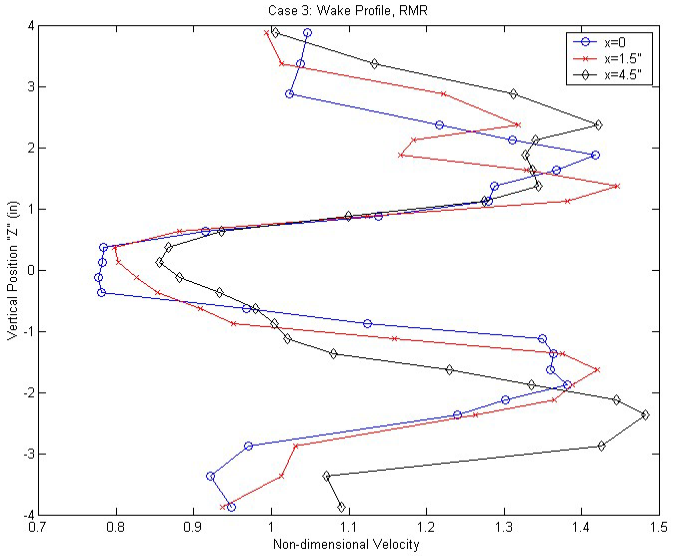

Figure 41. Wake Profiles for Case 3

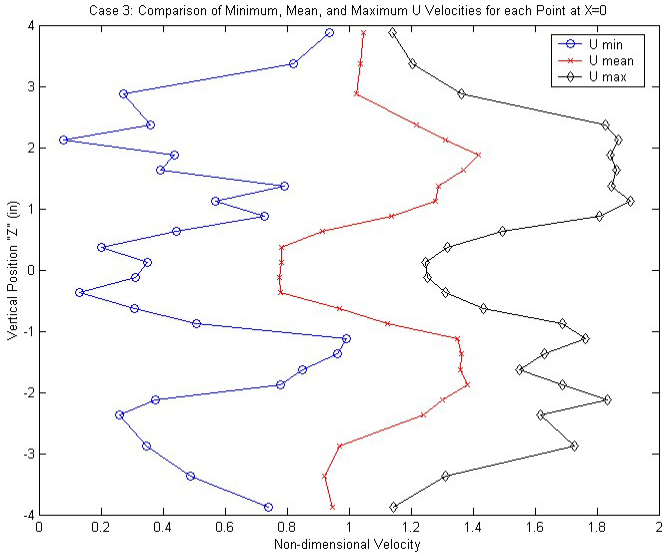

Figure 42. Minimum, Mean, and Maximum U Velocities at X=0, Case 3

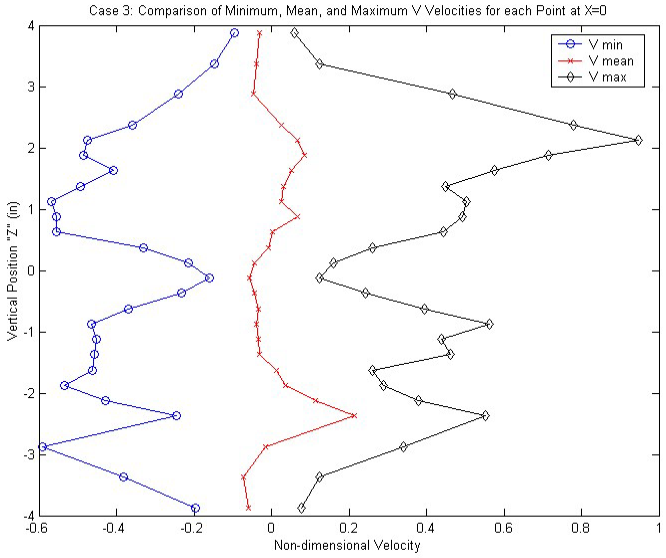

Figure 43. Minimum, Mean, and Maximum V Velocities at X=0, Case 3

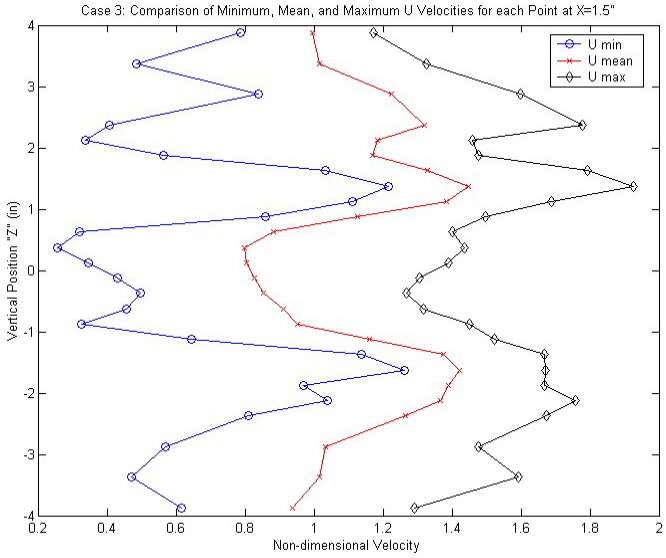

Figure 44. Minimum, Mean, and Maximum U Velocities at X=1.5”, Case 3

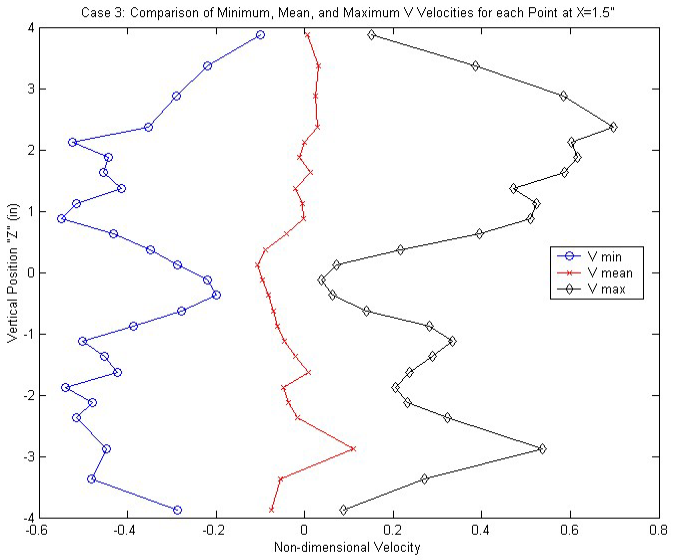

Figure 45. Minimum, Mean, and Maximum V Velocities at X=1.5”, Case 3

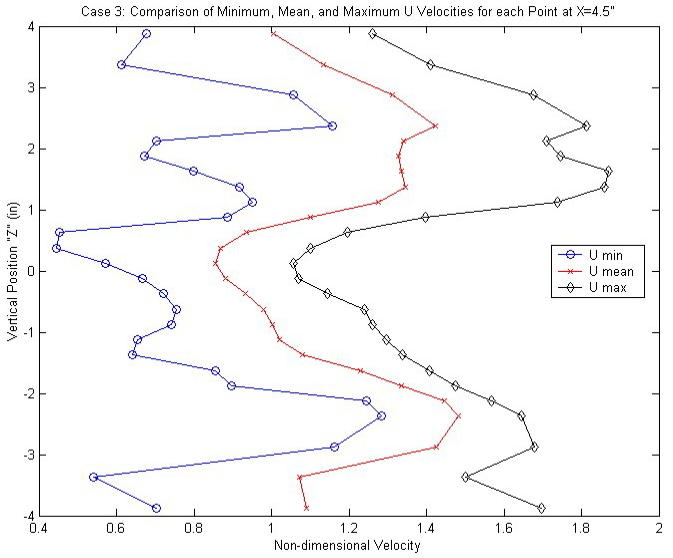

Figure 46. Minimum, Mean, and Maximum U Velocities at X=4.5”, Case 3

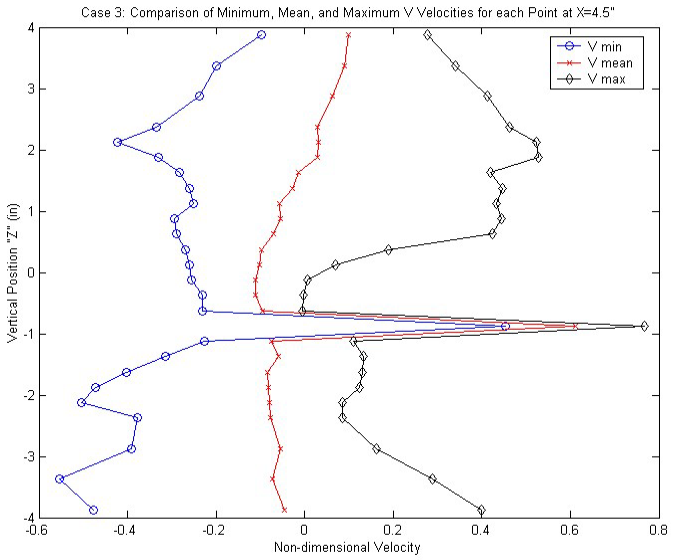

Figure 47. Minimum, Mean, and Maximum V Velocities at X=4.5”, Case 3

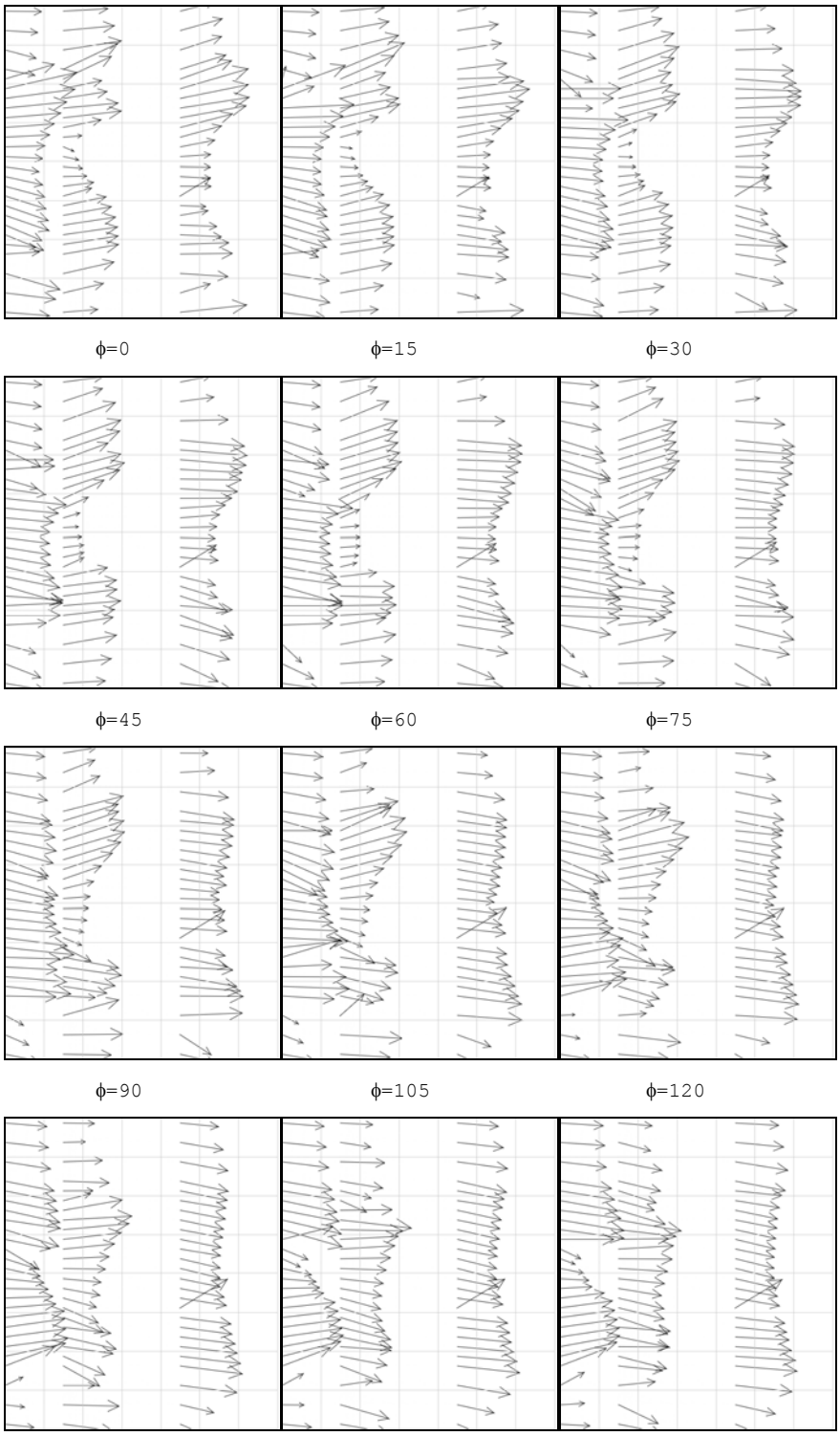

Figure 48. Case 3 Wake Profiles, 0-165°

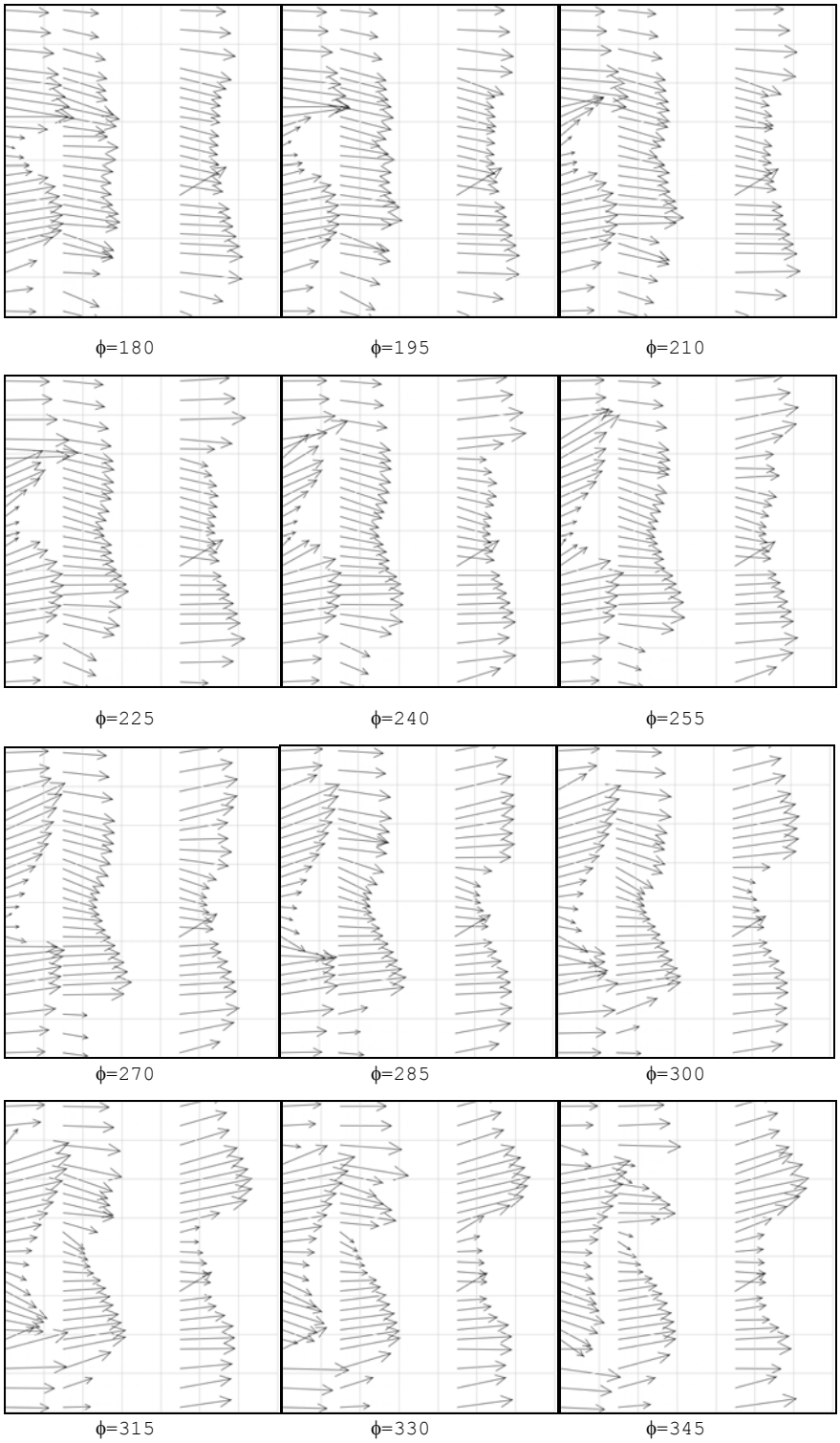

Figure 49. Case 3 Wake Profiles, 180-345°

APPENDIX E. PLOTS FROM CASE 4

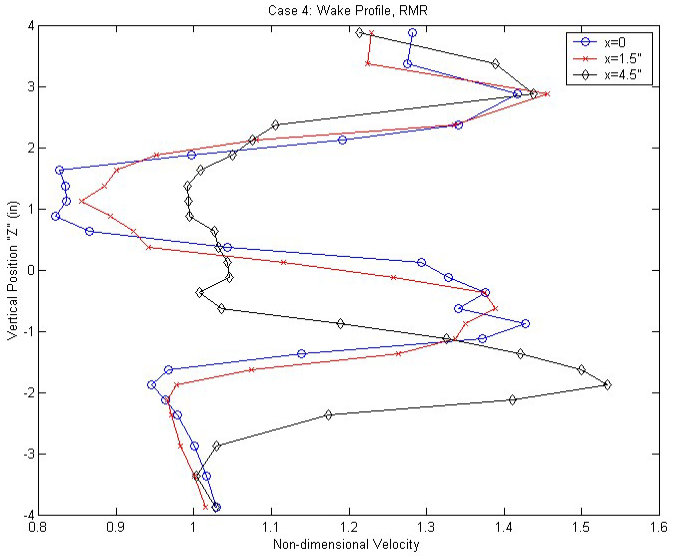

Figure 50. Wake Profiles for Case 4

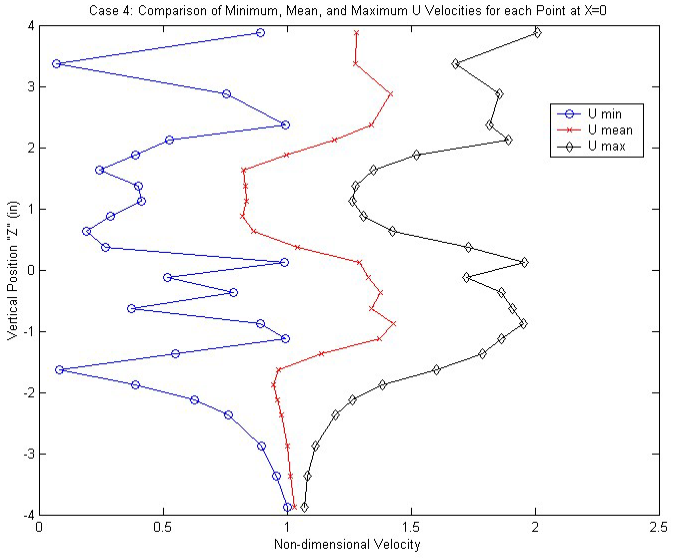

Figure 51. Minimum, Mean, and Maximum U Velocities at X=0, Case 4

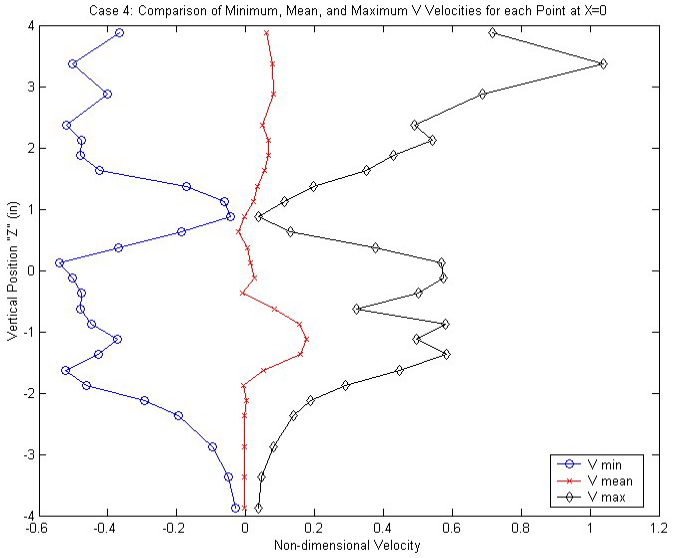

Figure 52. Minimum, Mean, and Maximum V Velocities at X=0, Case 4

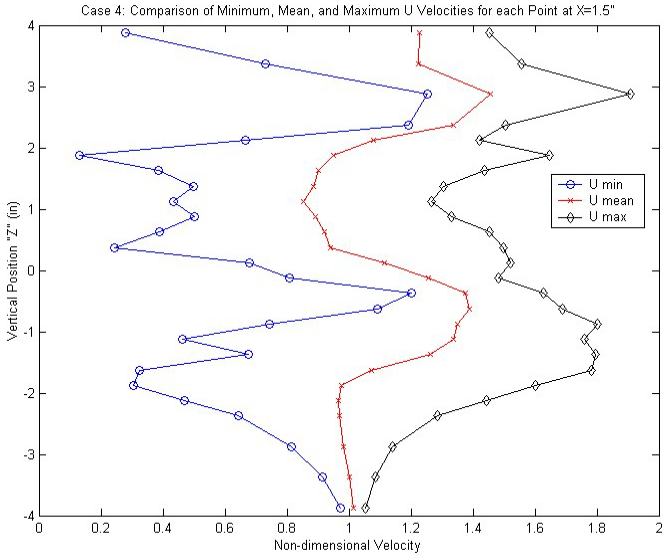

Figure 53. Minimum, Mean, and Maximum U Velocities at X=1.5”, Case 4

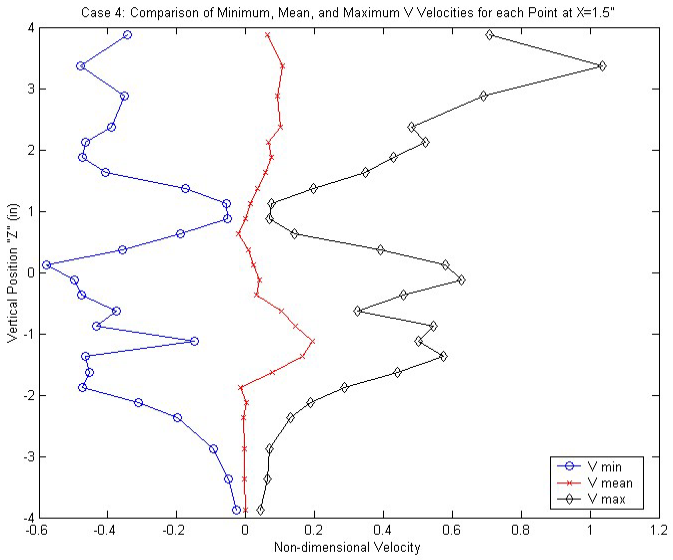

Figure 54. Minimum, Mean, and Maximum V Velocities at X=1.5”, Case 4

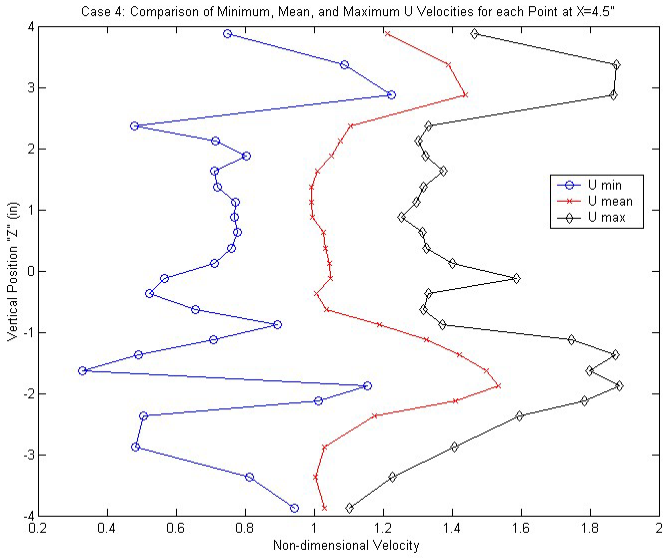

Figure 55. Minimum, Mean, and Maximum U Velocities at X=4.5”, Case 4

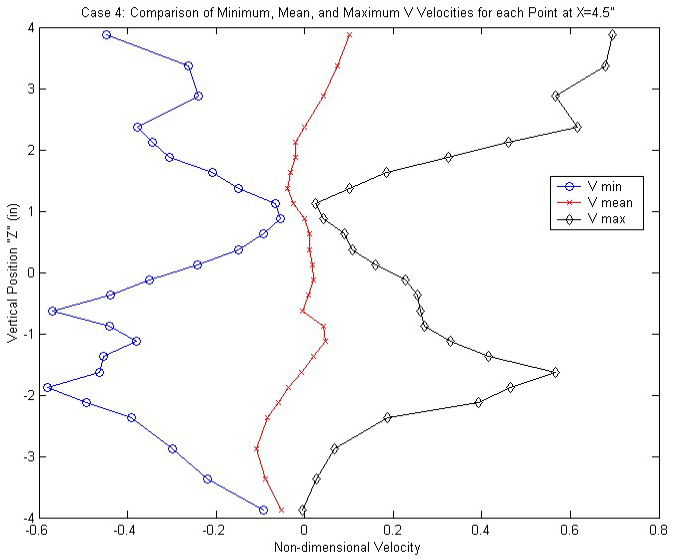

Figure 56. Minimum, Mean, and Maximum V Velocities at X=4.5”, Case 4

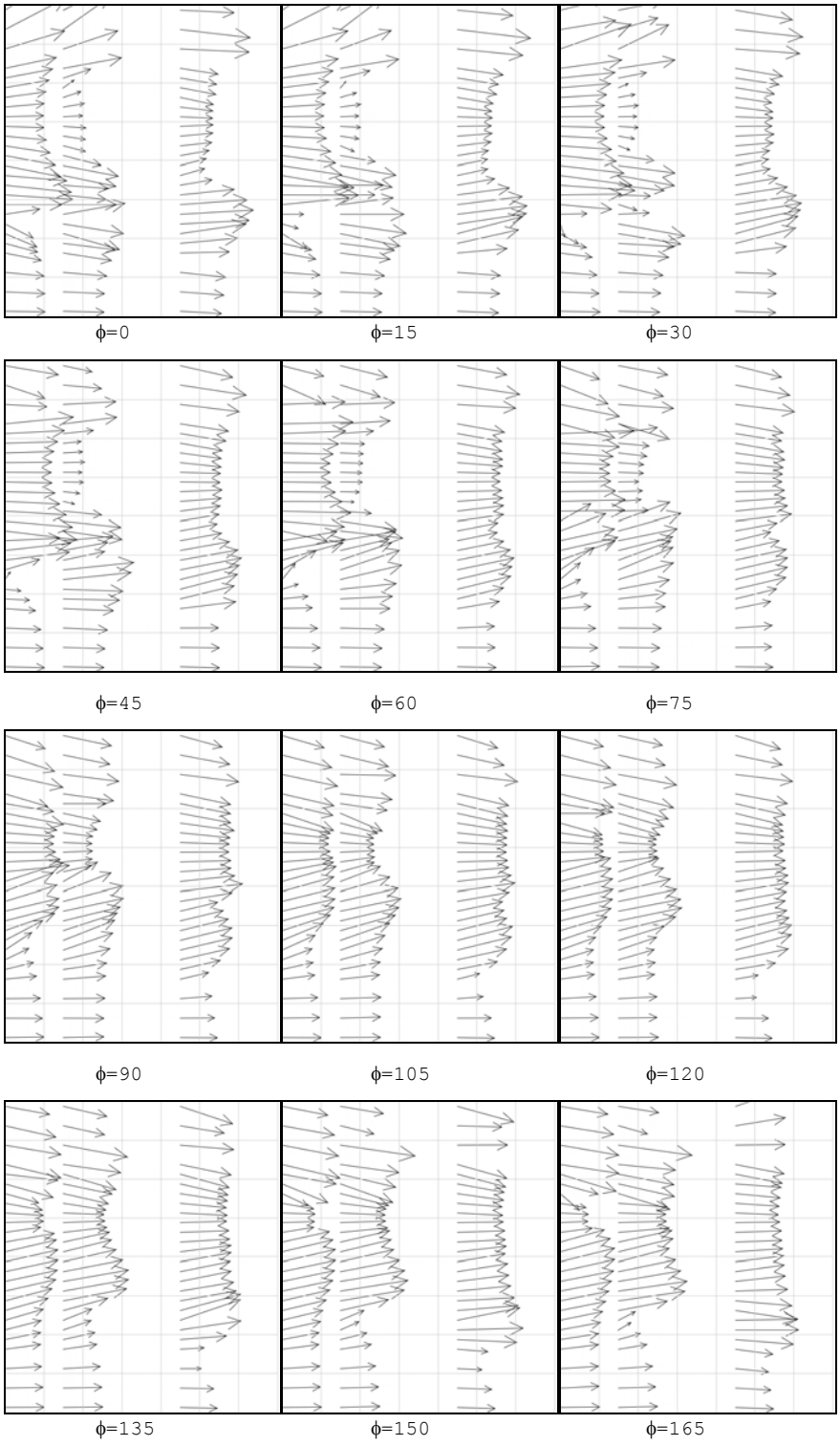

Figure 57. Case 4 Wake Profiles, 0-165°

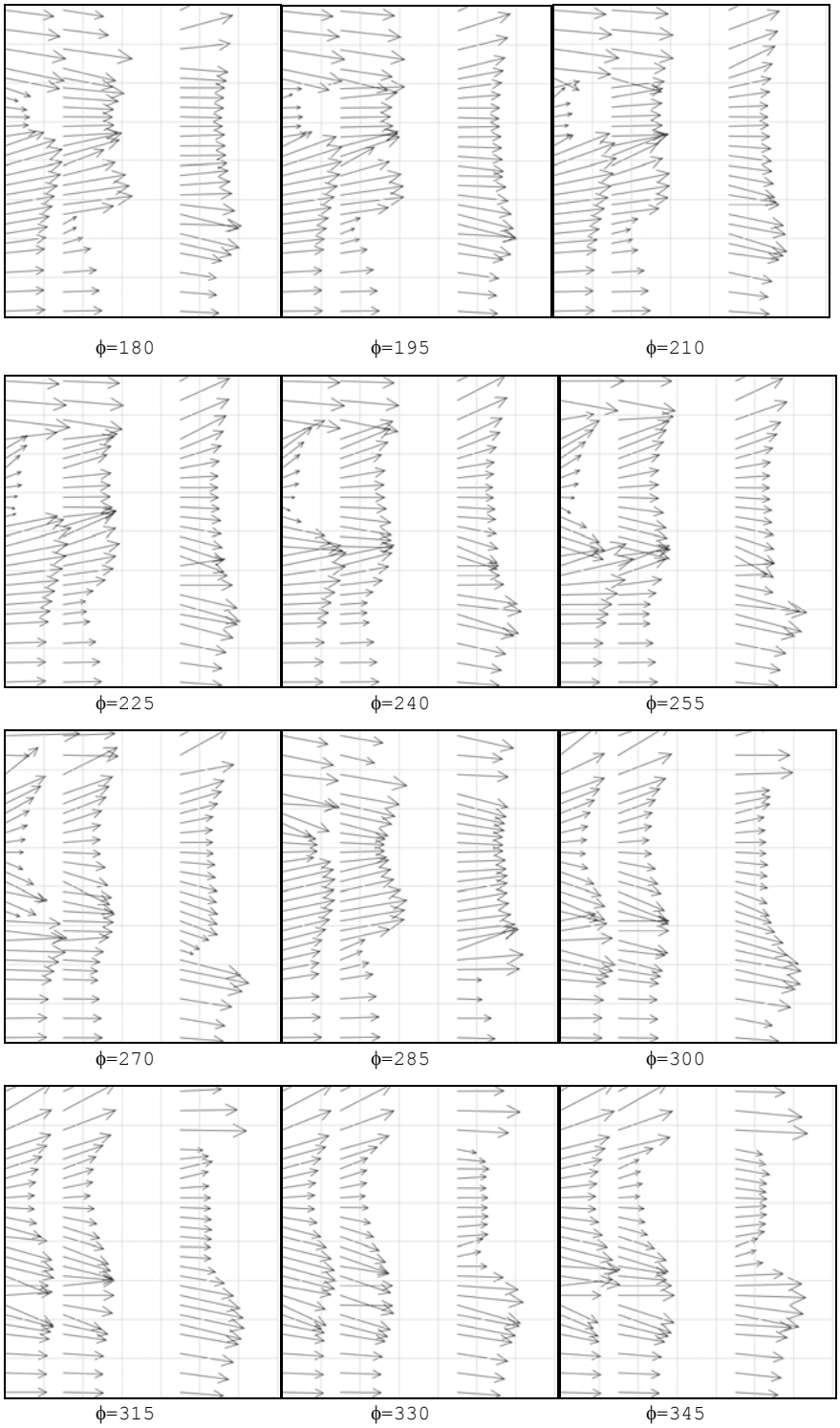

Figure 58. Case 4 Wake Profiles, 180-345°

APPENDIX F. PLOTS FROM CASE 5

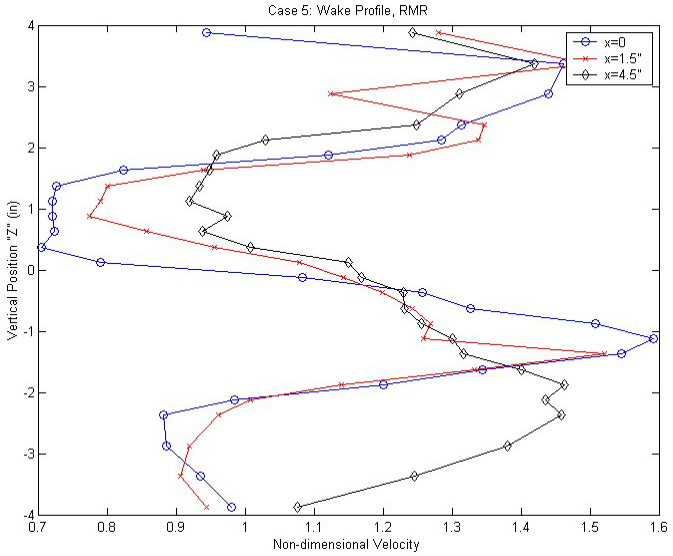

Figure 59. Wake Profiles for Case 5

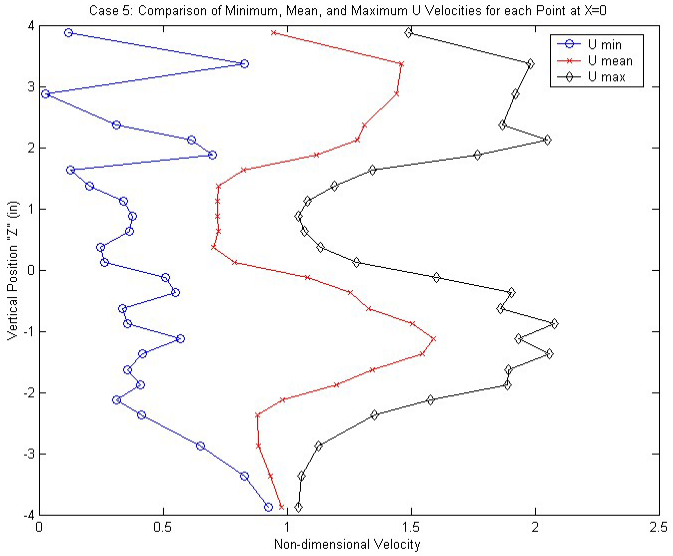

Figure 60. Minimum, Mean, and Maximum U Velocities at X=0, Case 5

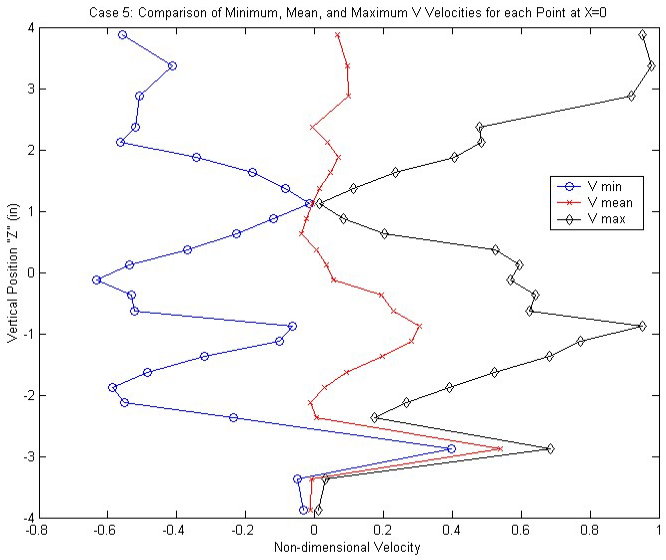

Figure 61. Minimum, Mean, and Maximum V Velocities at X=0, Case 5

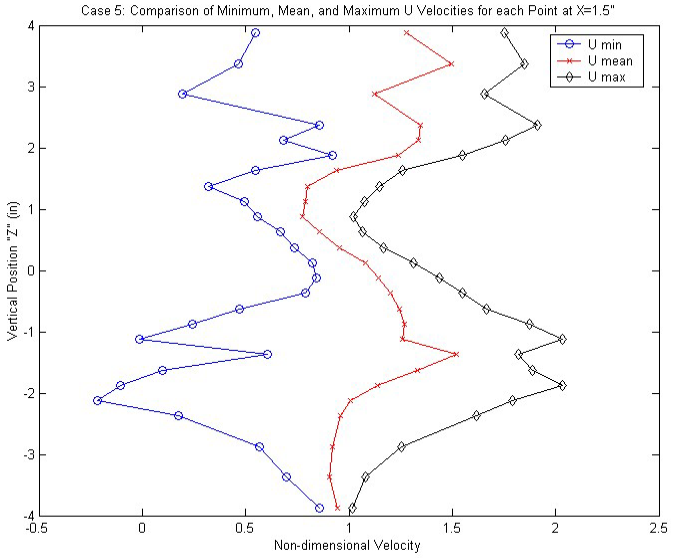

Figure 62. Minimum, Mean, and Maximum U Velocities at X=1.5”, Case 5

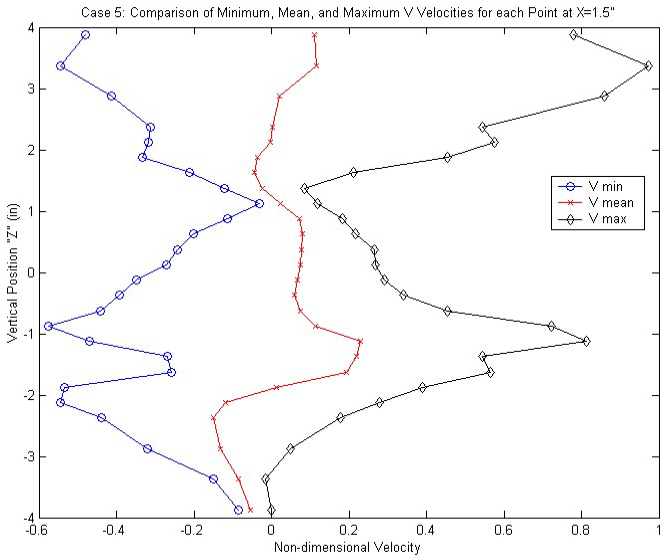

Figure 63. Minimum, Mean, and Maximum V Velocities at X=1.5”, Case 5

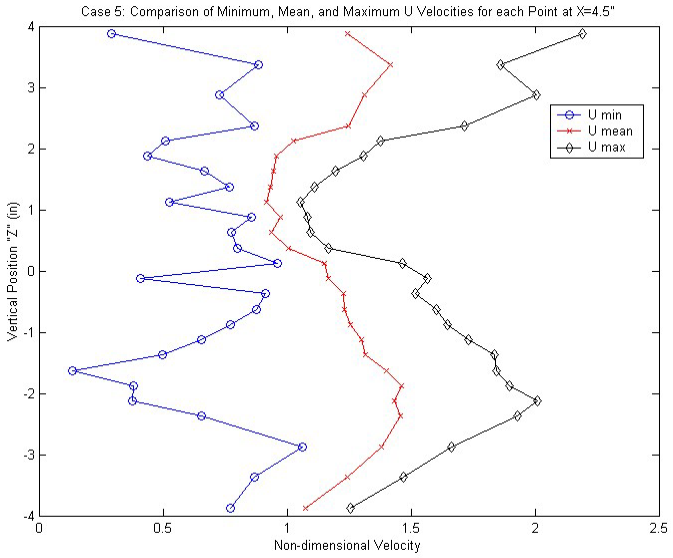

Figure 64. Minimum, Mean, and Maximum U Velocities at X=4.5”, Case 5

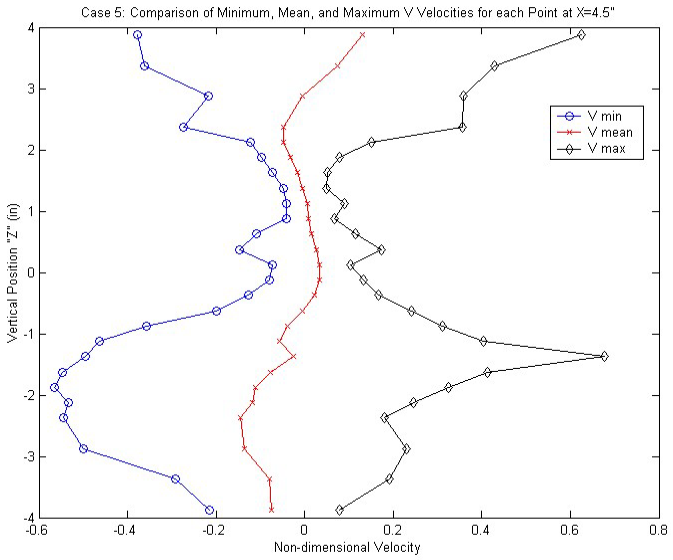

Figure 65. Minimum, Mean, and Maximum V Velocities at X=4.5”, Case 5

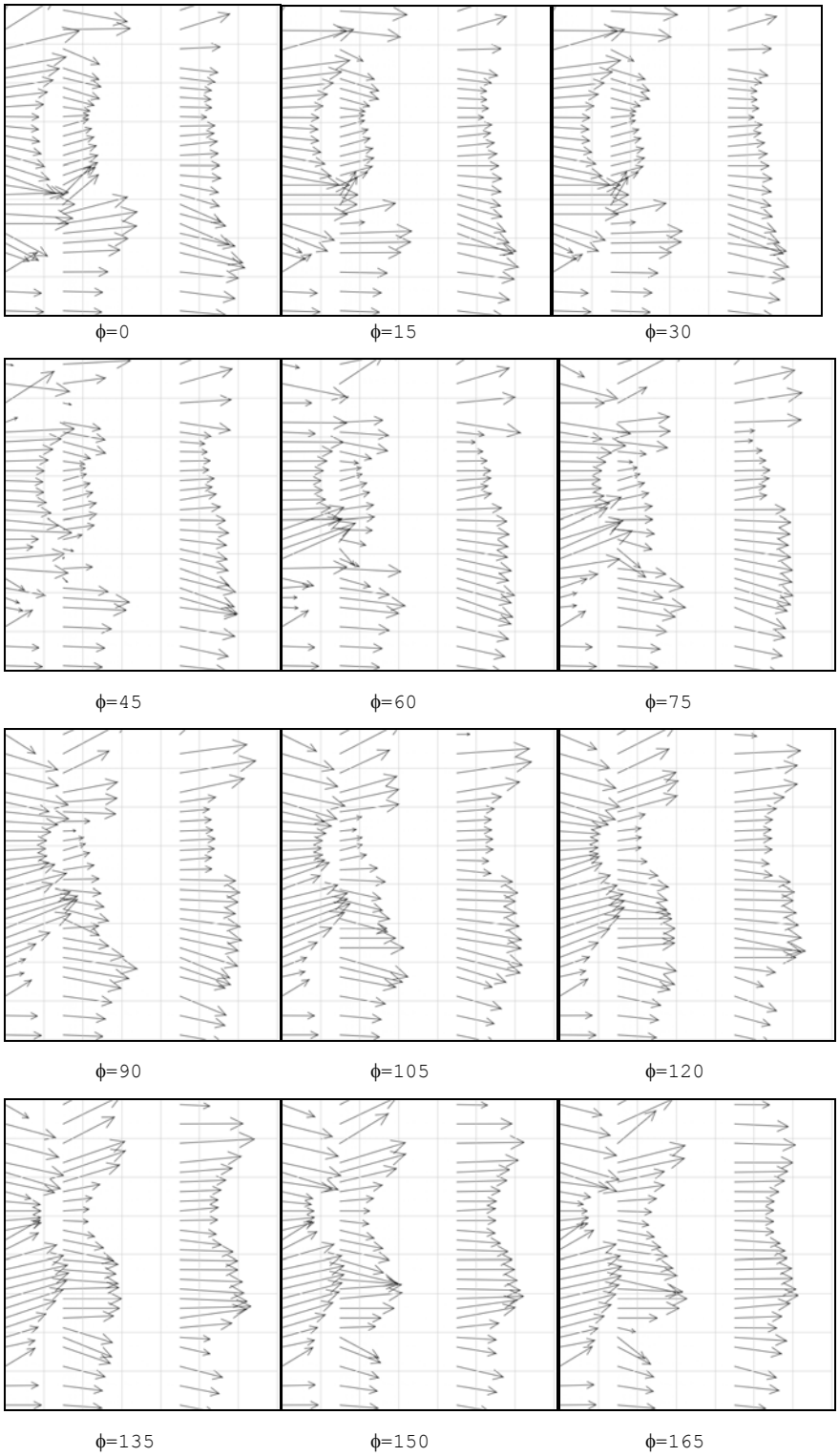

Figure 66. Case 5 Wake Profiles, 0-165°

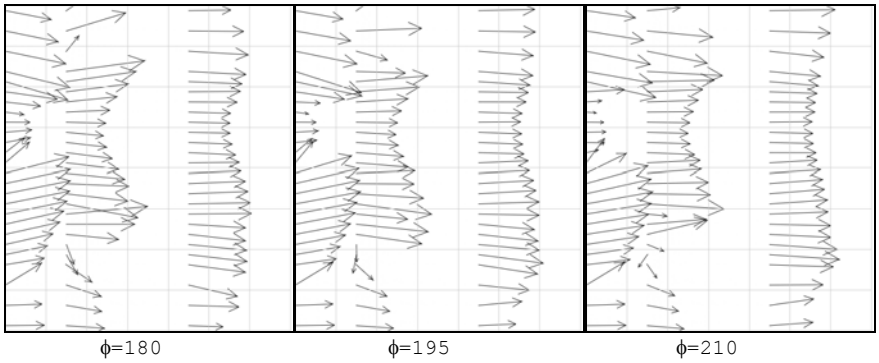

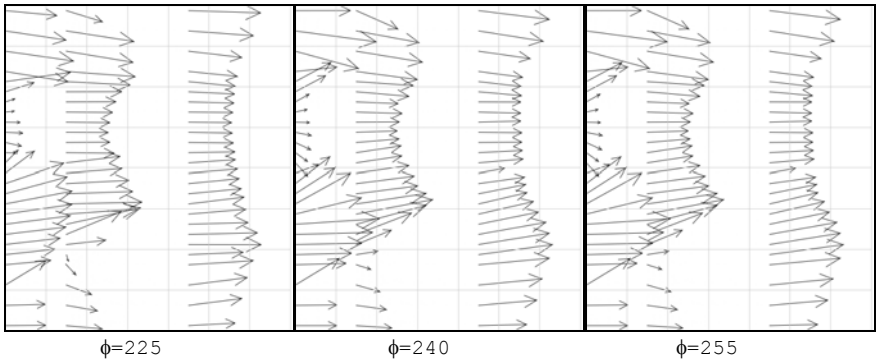

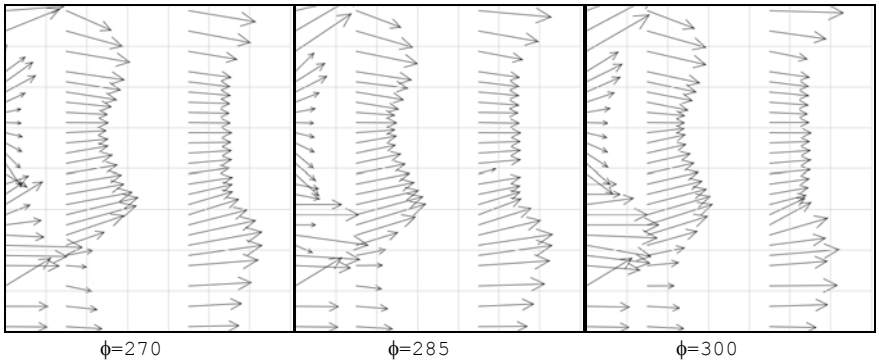

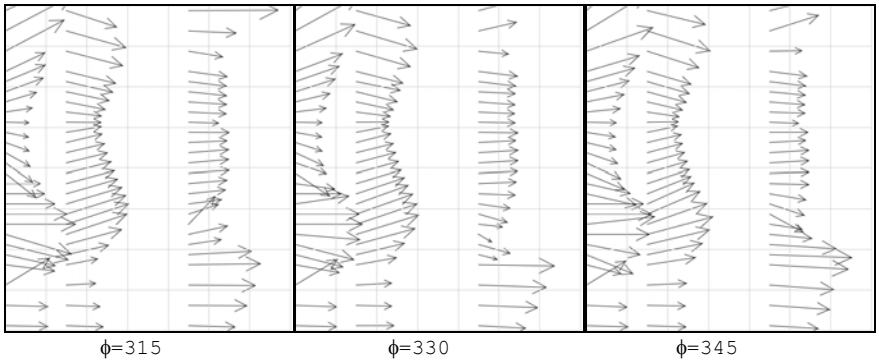

Figure 67. Case 5 Wake Profiles, 180-345°

APPENDIX G. PLOTS FROM CASE 6

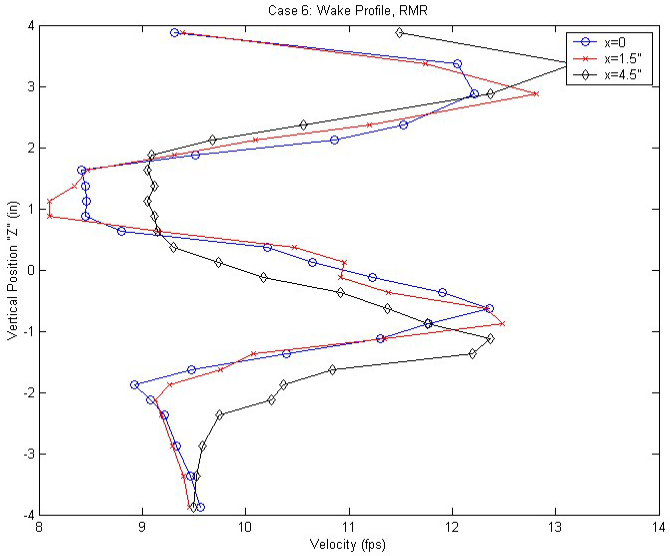

Figure 68. Wake Profiles for Case 6

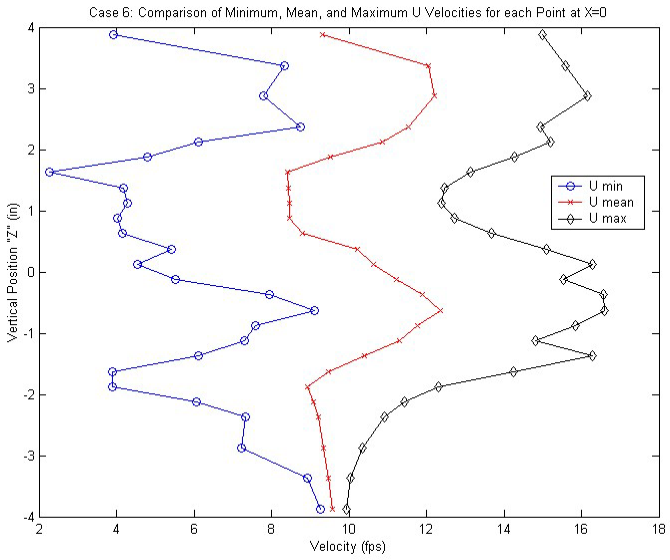

Figure 69. Minimum, Mean, and Maximum U Velocities at X=0, Case 6

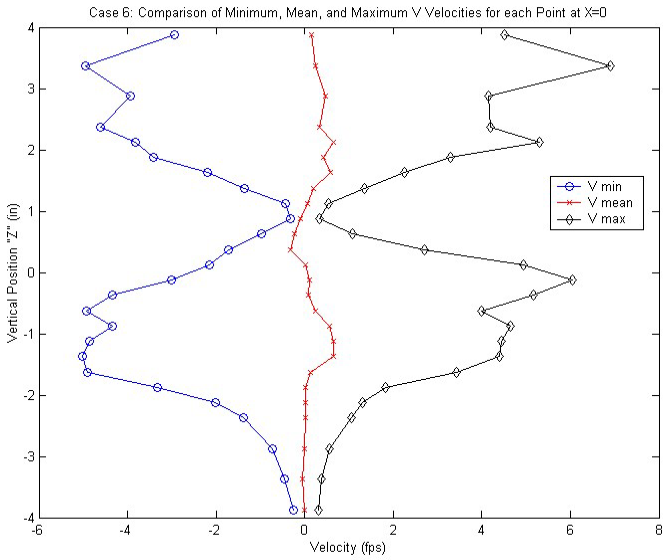

Figure 70. Minimum, Mean, and Maximum V Velocities at X=0, Case 6

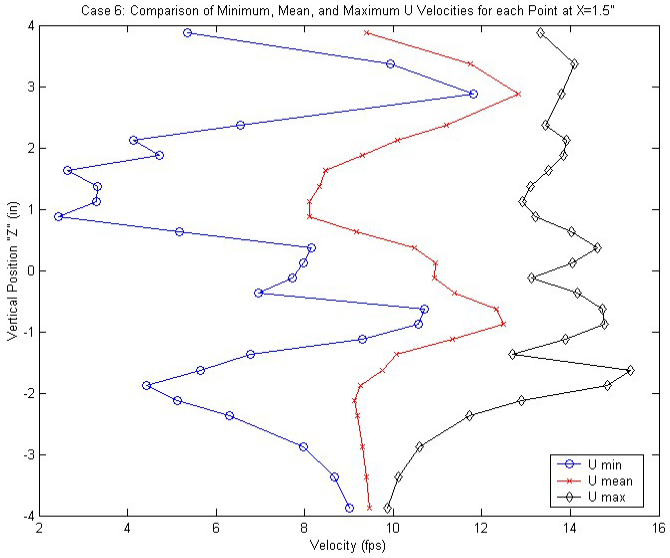

Figure 71. Minimum, Mean, and Maximum U Velocities at X=1.5”, Case 6

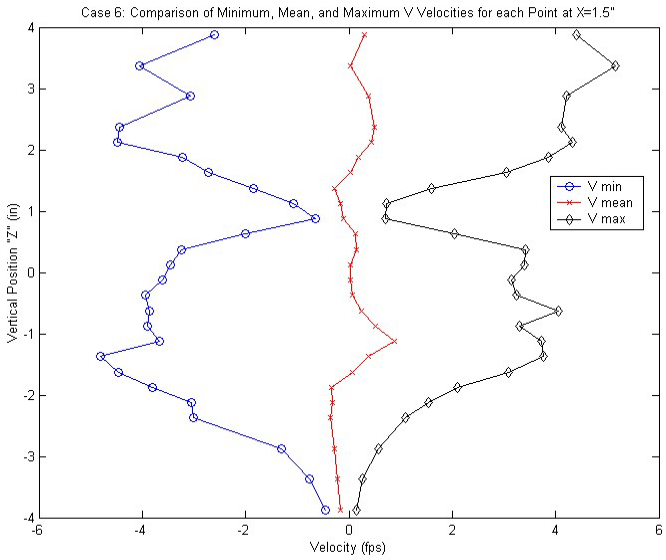

Figure 72. Minimum, Mean, and Maximum V Velocities at X=1.5”, Case 6

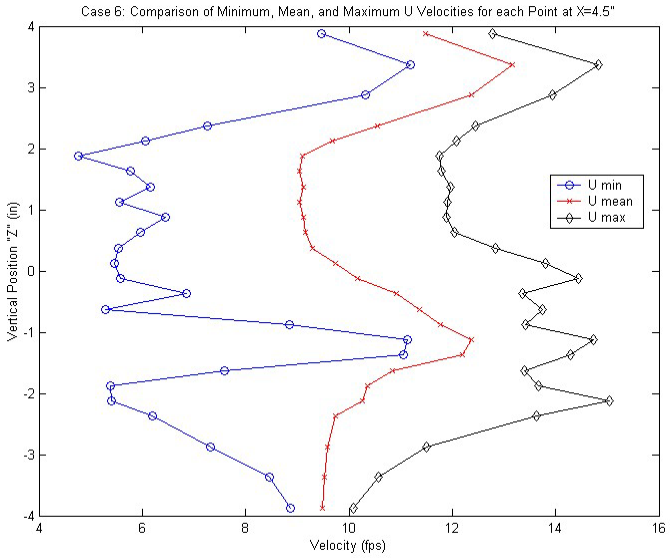

Figure 73. Minimum, Mean, and Maximum U Velocities at X=4.5”, Case 6

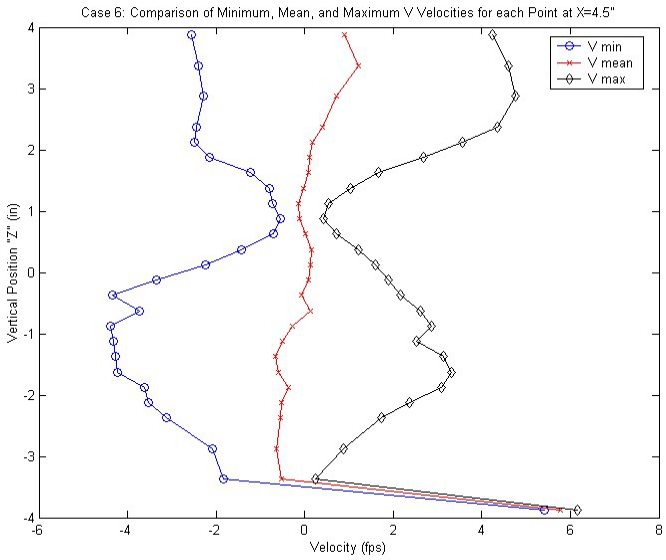

Figure 74. Minimum, Mean, and Maximum V Velocities at X=4.5”, Case 6

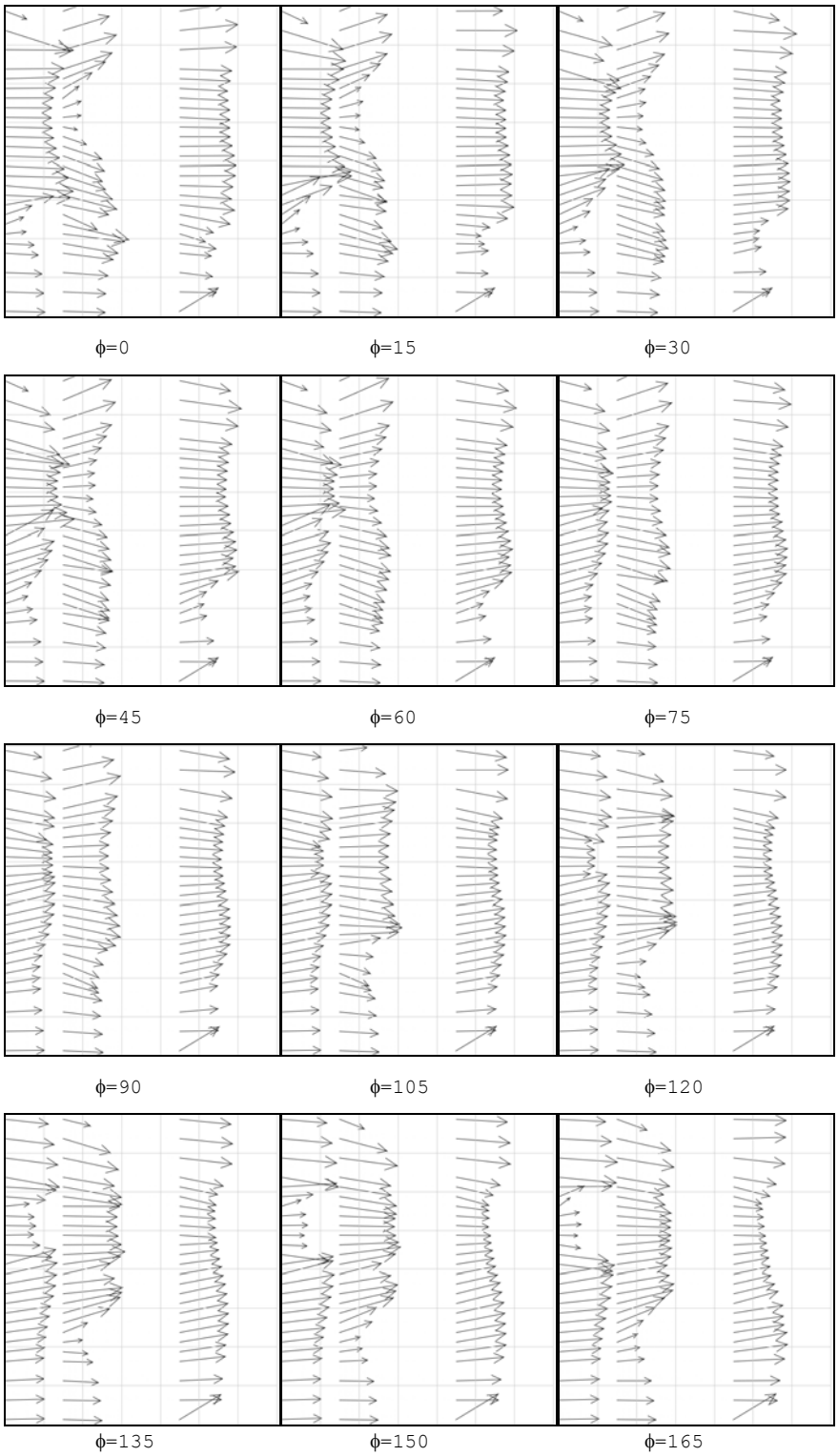

Figure 75. Case 6 Wake Profiles, 0-165°

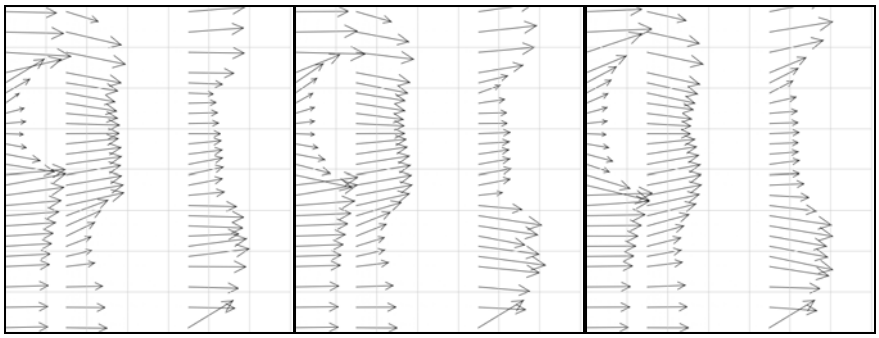

ϕ=180 ϕ=195 ϕ=210

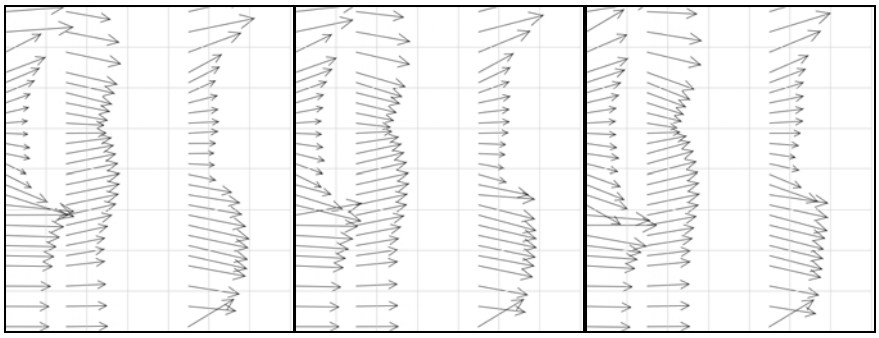

ϕ=225 ϕ=240 ϕ=255

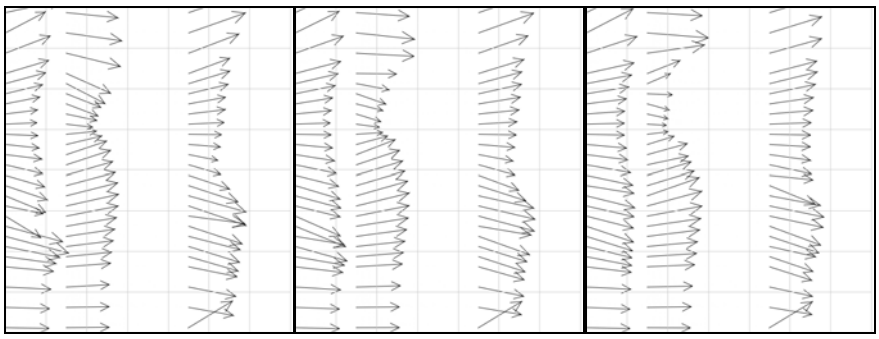

ϕ=270 ϕ=285 ϕ=300

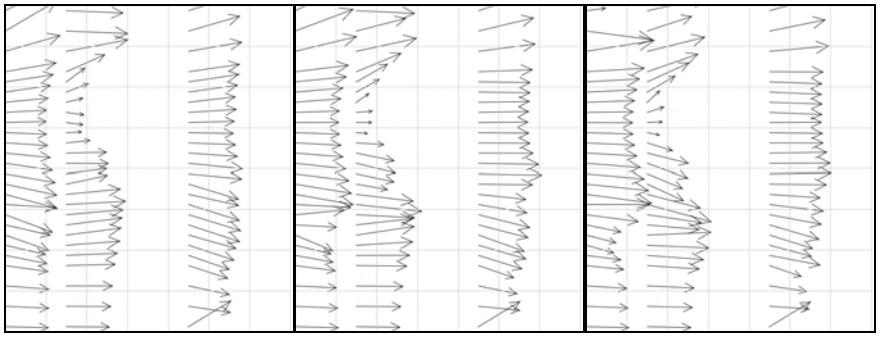

ϕ=315 ϕ=330 ϕ=345

Figure 76. Case 6 Wake Profiles, 180-345°

LIST OF REFERENCES

1. Duggan, S. "An Experimental Investigation of Flapping Wing Propulsion for Micro Air Vehicles." Naval Postgraduate School: June 2000.

2. Jones, K.; Duggan, S.; and Platzer, M. "Flapping Wing Propulsion for a Micro Air Vehicle." AIAA-2001-0126 8 January 2001.

3. Jones, K.; et al. "A Numerical and Experimental Investigation of Flapping-Wing Propulsion in Ground Effect." AIAA-2002-0866 8 January 2001.

4. Dohring, C.; Fottner, L.; and Platzer, M. "Experimental and Numerical Investigation of Flapping Wing Propulsion and Its Application for Boundary Layer Control." ASME 98-GT-46 2 June 1998.

5. Mueller, T and Zarchan, P., Ed. *Fixed and Flapping Wing Aerodynamics For Micro Air Vehicle Applications, Progress in Aeronautics and Astronautics Vol. 195.* AIAA, 2001

6. Lund, T. "A Computational and Experimental Investigation of Flapping Wing Propulsion." Naval Postgraduate School: June 2000.

7. Hedrick, S. "Unsteady Flow Field Measurements Using LDV." Naval Postgraduate School: June 1987.

8. www.roscoe-ca.com. *products: fog products: model4500*: June 2003.

THIS PAGE INTENTIONALLY LEFT BLANK

INITIAL DISTRIBUTION LIST

1. Defense Technical Information Center
   Ft. Belvoir, VA

2. Dudley Knox Library
   Naval Postgraduate School
   Monterey, CA

3. Professor Max Platzer
   Naval Postgraduate School
   Monterey, CA

4. Professor Garth Hobson
   Naval Postgraduate School
   Monterey, CA

5. Professor Muguru Chandrasekhara
   Naval Postgraduate School
   Monterey, CA

6. Professor Kevin Jones
   Naval Postgraduate School
   Monterey, CA

7. ENS Christopher J Bradshaw
   Naval Postgraduate School
   Monterey, CA